**University of Southampton**

Faculty of Engineering and Physical Sciences

# Developing an International Moth Testing Platform in a DVPP-Driven Real-Time Sailing Simulator

Thesis submitted in partial fulfilment of the requirements for the degree of

Master of Science in Maritime Engineering Science:
Yacht and High-performance Craft

---

**Luis Sampedro Moix**

**Supervisor:**
Stephen W. Boyd

**External Advisors:**
Gonzalo Redondo Dieguez | Ismael Iess Falcon | Ignacio Castañeda Sabadell

September 2025

# Declaration of Authorship

*This thesis was submitted for examination in September 2025. It does not necessarily represent the final form of the thesis as deposited in the University after examination.*

I, Luis Sampedro Moix declare that this thesis and the work presented in it are my own and have been generated by me as the result of my own original research.

I confirm that:

1. This work was done wholly or mainly while in candidature for a degree at this University;
2. Where any part of this thesis has previously been submitted for any other qualification at this University or any other institution, this has been clearly stated;
3. Where I have consulted the published work of others, this is always clearly attributed;
4. Where I have quoted from the work of others, the source is always given. With the exception of such quotations, this thesis is entirely my own work;
5. I have acknowledged all main sources of help;
6. Where the thesis is based on work done by myself jointly with others, I have made clear exactly what was done by others and what I have contributed myself;
7. None of this work has been published before submission.

# Acknowledgements

First, I want to thank the prestigious **Fundación Barrié** and its Overseas Postgraduate Scholarship Programme for sponsoring my Master's studies in Maritime Engineering Science: Yacht and High-Performance Craft at the University of Southampton. Thanks for believing in my project, passion and commitment. I will be forever grateful.

Next, I want to thank Joseph Ozanne, CEO of Simulator in Motion, and Gonzalo Redondo, CEO of D3 Applied Technologies, for providing access to their digital resources, their knowledge and, most importantly, their time. I would also like to thank my co-supervisors, Ismael Iess and Ignacio Castañeda, for their endless patience and guidance throughout this process. There could be no better teammates.

I would also like to thank Professor Stephen Boyd, my supervisor at the University of Southampton, firstly for giving his support when choosing the topic of the project, and secondly for his patience, trust, and guidance, which were invaluable in completing this project.

Separately, I would like to thank, in particular, Támara Echegoyen, Gonzalo Redondo, Marcos Míguez, my godfather Casto, and my father for all the help I received in gaining admission to the Master's program and securing the postgraduate scholarship; none of this would have been possible without each of them.

I want to thank my family and friends, especially my classmates at Boldrewood Campus, and Carlota, Jaime, Jovan, Luna, Martin, Robleda and Rodrigo, for their continuous support throughout my studies and for bearing with me during the stressful periods.

Finally, my thanks also go to the many others who, in one way or another, contributed to the successful completion of this stage of my career.

***A mis increíbles padres**: gracias. Desde la confianza y libertad que me habéis dado desde el primer momento, hasta los más mínimos detalles que hacen que todo esto sea por y para vosotros.*

# Abstract

The design of high-performance sailing craft has shifted from experience-driven iteration to data-driven workflows based on 3D modelling, computational fluid dynamics (CFD) and velocity prediction programmes (VPP). Hydro-foiling introduces inherently dynamic behaviours that exceed the scope of steady VPPs, motivating dynamic-DVPPs and simulators derived from them for design and training in America's Cup (AC) and other high-performance contexts.

This thesis implements an International Moth inside Simulator In Motion (SiM)—a DVPP-based sailing simulator—aligning geometry, mass properties and aero/hydro models, and establishing a workflow to compare predicted performance and controller behaviour across configurations. Simulations were executed in this independent environment, while D3-VPP® targets and the Exploder MD3 geometry supplied by D3 Applied Technologies, S.L. (D3) defined the reference conditions and baseline configuration. The work first benchmarks SiM against D3-VPP targets at two representative operating points (best-VMG upwind and downwind, TWS = 14 kn), then exercises two flight-control approaches: (i) a mechanical wand (sensitivities to gearing and wand length) and (ii) a heave PID (sensitivities to Kp, Ki and Kd), in flat water and a simple regular sea state.

The simulator reproduces the VPP targets within $\sim 1\%$ (speeds and VMGs), with attitudes close to target and force balances coherent at both points, supporting its credibility for controller studies in the tested envelope. For the wand, lower-response gearing attenuates wave-induced oscillations without degrading mean ride height, and increased wand length primarily biases the mean flight level while preserving a common steady wand angle. For the PID, a moderate tuning (baseline near $K_p \approx 4$, $K_i \approx 2$–$3$, $K_d \approx 6$) offers the best compromise between rise time and damping; relative to the wand the PID shortens settling and improves disturbance rejection in both flat and waves. Notably, electronic ride-height control is currently prohibited by the International Moth Class Rules, restricting such benefits to non-official contexts.

Overall, the platform meets its objectives: it (i) matches VPP targets credibly at 14 kn upwind/downwind, (ii) captures expected controller trends (gearing, wand length, PID gains), and (iii) provides a practical, repeatable bench for flight-control development. Future work should broaden the envelope (TWS/TWA and irregular seas), refine wand mechanism modelling, and test crew dynamics and manoeuvres.

**Keywords:** Dynamic Velocity Prediction Program (DVPP), Flight Control System, High-performance sailing, Hydrofoils, International Moth, Performance Data Analysis, proportional–integral–derivative controller (PID), Sailing Simulator, Simulator In Motion (SiM).

# Contents

# List of Figures

# List of Tables

# Nomenclature

## Acronyms

**AC** America's Cup; sailing competition and the oldest international competition still operating in any sport.. 1, 2, 23, VII

**AoA** Angle between a body's reference line and the incoming flow velocity vector. 16, 18, 37

**CFD** Computational Fluid Dynamics. 18, 20, 33, 38, 41, VII

**D3** D3 Applied Technologies, S.L. (website). 2, 3, 20, 25, 36, 39, 52, VII, XI

**DOF** Degrees of Freedom. 5, 9

**DVPP** Dynamic Velocity Prediction Program. 18, 22, VII

**FSI** fluid–structure interaction. 32, 33

**LE** Leading Edge; Forward edge of a foil or wing. Line that goes tip to tip. 32, 37

**LHS** See latin hypercube sampling (LHS). XVI

**LL** lifting-line theory. 32, 33

**PID** proportional–integral–derivative controller. 3, 4, 16, 25, 34, 48, 49, 51, 65, 75, 77, 81, 83, VII

**RANS** Reynolds-Averaged Navier-Stokes; CFD method that time-averages the flow and solves the mean field with a turbulence model (e.g. $k-\epsilon$, $k-\omega$). 5

**SiM** Simulator In Motion (website). 1–3, 25–27, 33, 35, 36, 39, 52, VII, XI

**TWA** True Wind Angle; the angle between the boat's heading and the direction of the true wind. ºDEG. 20, 35, XVI, XIX

**TWD** True Wind Direction; the direction from which the true wind is blowing, relative to north. ºDEG. 30, XVI

**TWS** True Wind Speed; the speed of the wind relative to the stationary ground, units of knots or m/s. 30, 42, VII

**VMG** Velocity Made Good; the component of a boat's velocity in the direction of the true wind, used as a measure of sailing efficiency. Kn. 11, 17, 18, 42, 57–66, 68, 71, XIX

**VMG** Speed of the sailing boat projected in the direction of the true wind (TWD). 20, VII

**VPP** Velocity Prediction Program. 2–5, 17, 21, 22, 66, VII

# Glossary

**aspect ratio** Relationship between the span of a foil and its chord. A high-aspect ratio wing has very long span and narrow chord and vice-versa. 10

**bias adjuster** Flight system control, that allows to effectively change the length of the push rod from the wand to the foil via an endless screw. It adjusts the ride height offset.. 16, 68, XVIII

**blade** See vertical. 32, XIX

**boom** Horizontal spar, attached at its forward end to the mast, used to extend and control the foot of the mainsail. XVIII

**chord** Straight-line distance between the leading edge and trailing edge of a foil, measured in the direction of the fluid flow. XVI

**design of experiments (DoE)** Statistical framework for planning runs to efficiently explore how inputs affect outputs. Common designs include full-factorial design, response-surface designs, orthogonal arrays and Latin hypercube sampling (LHS). 20

**downwind** Point of sail when the boat is sailing with the wind coming from behind, in moth sailing, the downwind condition encompasses broad reaching and running. 115° - 175° TWA. 10

**elevator** See horizontal. 32, XVII

**flat** Flattening coefficient of the sail profiles, directly related to the power generated by them, defined in the VPP. 20

**foiling** That uses a hydrofoil. 9, XVII

**forestay** Part of the standing rigging consisting of a wire or rope running from the upper front section of the mast to the bow of the boat, providing forward support for the mast. XVIII

**fluid–structure interaction** Coupled problem in which fluid loads deform or move a structure and the resulting motion alters the flow. XV

**full-factorial design** Design of experiments where all combinations of factor levels are tested. 20, XVI

**gantry** Aft structure projecting from the Moth transom that connects and transmits the forces of the rudder, situated aft of the hull, it increases pitch lever arm.. 32, 37

**gearing** key parameter that controls the ratio between wand angle and flap angle in the moth flight system. The sailor can touch the gearing while sailing, from position 1 to 6, to control how the boat behaves in waves. See § 2.3.5 and Fig. 5.2 for system description and § 5.3 for influence. 3, 14, 16, 34, 51, 55, VII

**gradient descent** Iterative optimisation method that updates parameters in the direction of negative gradient of the objective. 20

**horizontal** Horizontal lifting surface; on the mainfoil called the wing, on the rudder the elevator; generates lift or downforce for heave/pitch control. 20, 32, 33, 37, XVI, XIX

**hydrofoil** A lifting surface, i.e. "foil", e.g. a horizontal wing, that operates in water to raise the vessel's hull above the free surface. VII, XVI

**International Moth** 3.35-metre-long sailing foiling monohull, built in carbon fibre under the International Moth class rule, recognised by World Sailing. See 2.3. 1, 25, VII, XVIII

**Kd** Derivative gain. Scales the error's time derivative to add damping and anticipate changes; sensitive to measurement noise. 35, 51, 75, 79, 80, VII

**Ki** Integral gain. Scales the time–integral of the error to remove steady–state offset; too large may cause windup and oscillations. 35, 51, 75, 78, 80, VII

**Kp** Proportional gain. Scales the instantaneous error $e(t)$ to increase responsiveness; excessive values can amplify noise or overshoot. 35, 51, 75, 77, 80, VII

**latin hypercube sampling (LHS)** Sampling scheme that divides each input dimension into equal-probability bins and samples each bin exactly once per dimension. 20, XV

**lifting-line theory** Mathematical model that predicts lift distribution over a three-dimensional finite wing/foil in inviscid, incompressible flow to compute circulation, lift distribution and induced drag (best for thin, moderately loaded, high-aspect-ratio foils). 32, 33, 36, 48, XV

**line search** basic iterative approach to find a local minimum of an objective function along a given descent direction (e.g., gradient). 52

**mainfoil** Front T-hydrofoil assembly in the Moth (aka *main*); provides most of the vertical lift.. 56

**mainsail** The principal and typically largest sail on a sailing vessel, set aft of the main mast and attached along its luff to the mast and along its foot to the boom. In the case of the moth it is the only sail used (in opposition to other types of vessels with, e.g., mainsail and headsail). XVI

**monohull** A type of vessel characterized by a single main hull, as opposed to multihull designs such as catamarans or trimarans. XVII

**moth** See International Moth. 3, 9, 10, XVIII

**perturbations method** Sensitivity method that varies a single input slightly around a baseline to estimate its effect. 20

**rake** angle of rotation on the local Y-axis (horizontal and transversal to the sailboat) of the different movable elements on-board. 12

**ride height offset** neutral flap angle bias. Sailors adjust this control to achieve the desired ride height, after selecting the desired wand length and gearing. See bias adjuster. 16, XVI

**rig** The set of mast plus sail(s) plus associated elements, e.g., in the moth: shrouds, forestay and boom. 10

**rudder** Aft steering appendage; on the moth it carries a horizontal *elevator* that adds pitch stability and trim authority. 10, 12

**sailplan** Arrangement of the sails and spars of a sailing vessel, defining its rig type and sail area distribution. 11

**shroud** Part of the standing rigging consisting of wires or ropes running from the mast to the sides of the vessel to provide lateral support and keep the mast upright. XVIII

**span** Tip-to-tip distance across a foil, measured perpendicular to the direction of the flow. XVI

**strut** See vertical. 32, XIX

**upwind** Point of sail when the boat is heading as close to the wind direction as possible (close-hauled), for the International Moth, the best-VMG lies between 35º – 50º TWA, almost a close reaching. 10

**vertical** Vertical member of a hydrofoil (also strut in case of the mainfoil; or blade on the rudder); connects hull to the horizontal surface and transmits loads. 20, 32, 37, XVI, XIX

**vortex lattice method** Potential-flow panel method that discretises the lifting surface into an infinitely thin sheet of discrete vortices; the influence of the thickness and viscosity is neglected. 36

**wand** Carbon fibre rod that touches the water and through a linkage system (gearing and offset), it transmits a control input to the foil flap.. 3, 5, 14, 34, 49, 51, 66, VII

**wing** See horizontal. 32, XVII

**World Sailing** The governing body of sailing worldwide, formally known as the International Sailing Federation (ISAF). XVII

# 1.

# Introduction

Testing and developing new components for foiling and high-performance boats is both risky and costly. The ever-changing wind and wave conditions make it very challenging to compare sailing performance consistently. There is a clear need for a new testing method that accounts for dynamic effects and environmental factors. What if we could apply the state-of-the-art simulators used in the America's Cup (AC) to the world's fastest and most advanced dinghy: the International Moth?


Figure 1.1: International Moth completely assembled sailing inside the SiM environment

## 1.1 Aim and Motivation

The implementation of new hydro-foiling technology in sailing yachts over recent years has brought new challenges. For example, traditional Velocity Prediction Programs (VPP) no longer accurately describe the dynamic nature of foiling. It has been necessary to advance further and to develop time-domain Dynamic-VPPs [1].

In the 37th America's Cup, the use of sailing simulators that seamlessly integrated design development, mechatronics testing, crew training, and virtual racing, built inside Simulator in Motion, established simulation not as an option, but as a mandatory path to engineering excellence [2].

The International Moth Class (a 3.35-metre-long sailing foiling monohull, built in carbon fibre) has a set of Rules [3] that establish a set of dimensional, design, and performance restrictions to promote real-time racing competition among boats designed by different shipyards and designers.

This thesis aimed to develop a digital model of the International Moth dinghy under the International Moth Class Rules inside a sailing simulator (Simulator in Motion® 's (SiM) platform) based on a Dynamic-VPP. This advanced tool is able to integrate multiple physics models and compute the force equilibrium in real time. For achieving these objectives has been essential the collaboration of D3 Applied Technologies, S.L. (D3), a yacht design company experienced in America's Cup campaigns that has developed a D3-VPP and provided access to the SiM platform.

The participation of D3 and Simulator in Motion in this project makes it as state-of-the-art as it can be, as of today (2025). The access to the SiM tool opens the opportunity to test multiple configurations and develop initial methods of analysis that would be useful in the future, and challenging to create without the data that the SiM provides.

## 1.2 Scope and Limitations

This project has been built around the primary objective of establishing a robust testing platform for an International Moth through the correct use of the Simulator in Motion. Once this primary objective was achieved, efforts had to be directed towards a more specific analysis. The use of a simulator as a test bench opens up an enormous range of possibilities, since it allows virtually any aspect to be tested — for example, different foils or the boat's sensitivity to changes in particular variables such as heel. To produce a final project that genuinely requires a simulator, the decision was made to focus on a single analysis that could exemplify the numerous potential applications once the test bench is created. This example had to be something that could not be carried out solely with a VPP — such as a sensitivity study to state variables (e.g. heel), or finding the optimal upwind condition, both of which are studies well-suited to be done with a VPP.

Therefore, the analysis focused on modelling the International Moth mechanical flight control system as faithfully as possible, and on assessing its sensitivity to changes in different parameters and in the surrounding environment.

As this is a MSc Final Research Project, the complete development of the moth platform in the simulator, together with an extensive analysis of its performance, exceeds the scope, time and objective of this thesis. Thus, some limitations have been established:

i Simulations will be analysed and compared in the absence and presence of a single model wave, even though the simulator can add any seastate desired.

ii Only two sailing points will be used in testing (upwind and downwind VMG target)

iii We assumed some physics limitations in the physics models present in the SiM (see § 3.3).

iv PID optimisation was paused when a stable flying Moth dynamics was obtained. The three PIDs would benefit from further, more precise tuning.

v The results presented in Chapter 5 are only the ones considered as the most relevant. The simulator tool produces extensive and detailed outputs; however, analysing and presenting all of them for all the number of tests done is out of the scope of this project.

## 1.3 Specific Objectives

Looking for an efficient use of time and resources, three specific objectives were defined for this Thesis:

**O1** To build a testing platform inside the SiM that works seamlessly and can obtain similar performance metrics as the D3-VPP, with the help of three PID's (heel, TWA, heave). Test the extent to which sailing behaviour corresponds to reality and improve the PID variables until a stable platform is achieved.

**O2** To model a mechanical Wand Flight Control System inside the SiM simulator to be able to test how different variables like the gearing or the wand length affect the flying behaviour and boat performance, using as response variables height of flight (vertical foil immersion), wand angle and VMG.

**O3** To compare the behaviour of both the designed PID-controlled and the Wand-controlled flight systems and conclude the benefits and drawbacks of each system.

## 1.4 Overview

To ensure a coherent and logical flow, this MSc Final Project was divided into six chapters. The document is organised as follows:

**Chapter 1**

**Introduction**. This chapter provides initial insights into what the project aims for, motivation and scope.

**Chapter 2**

**Background**. Summarizes the information necessary for understanding the motivation and the relevance of the objective based in an adequate literature review; establishes the fundamentals for understanding sailing principles to readers not familiar with it; and provides valuable material about VPPs and sailing simulators to fully understand the more technical part of the document (Chapters 3, 4, 5 and 6).

**Chapter 3**

**Methodology for Modelling, Control, and Simulation**. Describes the steps of the research in a time-logical sequence. Additionally, it introduces the Simulator in Motion platform, detailing the assembly of the testing platform and how the required physics models were implemented.

**Chapter 4**

**Assessing that the SiM outputs are consistent with VPP targets**. This chapter benchmarks the Simulator-in-Motion (SiM) outputs against targets from the D3 Velocity Prediction Program (D3-VPP) at two representative operating conditions (upwind and downwind at TWS = 14 kn).

**Chapter 5**

**Developing a Flight Control System for the International Moth Simulator**. In this chapter, two different flight control systems are developed and compared, with their key variables studied through various tests. One flight control system is based on a PID, and the other is based on a mechanical wand. This chapter contains the analysis, results and conclusions of 4 different studies:

- Gearing Sensitivity Study
- Wand Length Sensitivity Study
- Heave PID Controller Study
- Comparison between the Wand Mechanism and the heave PID

**Chapter 6**

**Conclusions**. Here, the key conclusions of the entire project are gathered together.

# 2.

# Background and Literature Review

Hydrofoils, by lifting the hull out of the water, produce extreme changes in the forces and dynamics of sailing boats. When the foils provide sufficient vertical lift, the wetted area and wave-making drop significantly, leading to improved speed and comfort. In this foiling regime, the critical physics also change: heave, pitch and roll couple strongly with foil angle of attack, free-surface effects and the control inputs from the sailor.

Classical VPPs are still very useful for layout, trade-offs and polars, but they assume steady state. Things like take-off, ride-height control, porpoising and manoeuvres need a time-domain view. In this project, we use both a VPP to define reasonable operating points and targets, and a 6-DOF dynamic model (simulator) to study stability and the effect of the (mechanical) controllers on a foiling dinghy.

The International Moth is a good case study because it is very sensitive. Small-scale, high-aspect-ratio appendages and fully mechanical flight control (wand–flap and rudder-rake) make apparent-wind build-up, ride height, and foil incidence critical. Below, we provide a brief historical context, followed by an introduction to the sailing mechanics and the Moth flight-control system used later in the VPP and simulator.

## 2.1 A short historical note on hydrofoils

Early trials already showed the idea clearly: swap buoyancy for lift to cut drag. In the 1860s, Thomas Moy towed small "winged" models on London canals and noted the craft lifting out of the water [4]. A few decades later, Forlanini tested full-scale ladder foils on Lago Maggiore and reached high speeds for the time [5]. Meacham's 1906 article explained the principles to a broad audience, and, soon after, Bell and Baldwin's HD–4 set a water-speed record of 70.86 mph (1919) [6], [7].

After WWII, navies explored fixed-foil craft, and by mid-century, reviews were already discussing the advantages and limits of hydrofoil-supported boats [8]. With modern computational advances, designers moved from simple potential-flow ideas to panel methods and then to RANS, which allowed more systematic study of 2D/3D hydrofoils near the free surface, shallow submergence and non-linear effects. Good summaries of this evolution and its application to planing/high-speed vessels are given in recent reviews [9] and in standard yacht-design texts [10].

## 2.2 Sailing Mechanics Background

The first step to define the behaviour of a sailing yacht is to determine the Wind Triangle and then establish the equilibrium.

In this section, the interaction of the hydro- and aerodynamic forces generated on the different elements of the yacht will be explained, along with the necessary definitions.[10]

### 2.2.1 The Wind Triangle

The aerodynamic behaviour of a yacht cannot be understood without first introducing the so-called *velocity triangle*. This representation relates the true wind velocity, the yacht's forward speed, and the apparent wind experienced by the sails. The apparent wind direction and intensity are decisive, since the sails act as aerodynamic profiles that generate lift and drag with respect to this apparent flow.

Figure 2.1 illustrates the velocity triangle, showing how the apparent wind results from the vector addition of the true wind and the boat velocity. This apparent wind is the one that actually governs the aerodynamic loading of the sails and thus the forces transmitted to the hull.[10], [11]

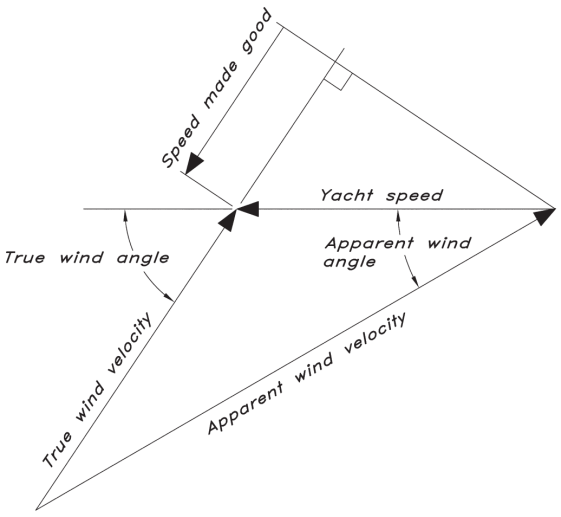


Figure 2.1: The velocity triangle of a sailing yacht. Adapted from [10].

### 2.2.2 XY equilibrium

Once the aerodynamic forces are defined, the equilibrium of the yacht in the horizontal plane can be analysed. The sail forces can be decomposed into lift and drag components with respect to the apparent wind, which are then projected into the boat-fixed reference frame (surge, sway, and yaw).

The balance in the XY plane is essentially a trade-off between the aerodynamic driving force and the hydrodynamic resistance of the hull and appendages. The lateral component of the sail force (side force) must be countered by the keel and rudder, generating lift to oppose leeway. At the same time, a yawing moment is created depending on the relative positions of the sail force centre and the underwater centre of lateral resistance. This moment is controlled mainly through rudder angle and crew trim.[10], [12]

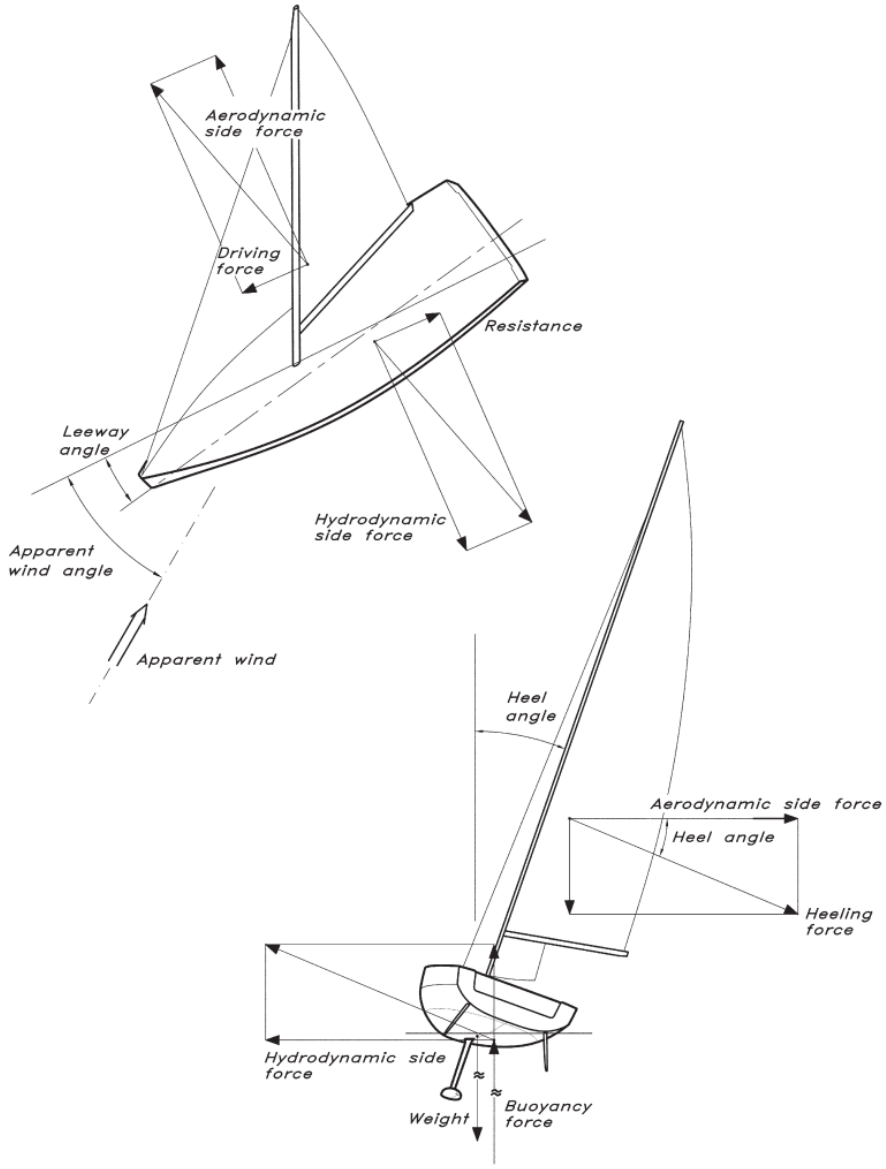


Figure 2.2: Aerodynamic and hydrodynamic forces on a sailing yacht. Adapted from [10].

### 2.2.3 YZ equilibrium

In the vertical plane, equilibrium involves the interaction between the aerodynamic heeling moment and the righting moment generated by the hull, keel and crew weight. The

aerodynamic forces acting above the waterline create a moment that tends to heel the yacht, while the hydrostatic and dynamic righting arms resist this motion.

For conventional displacement yachts, the equilibrium in this plane can be described using traditional hydrostatic formulations of righting arm curves and heeling moments.[10], [12]

### 2.2.4 International Moth

The foiling moth is a complex, three-dimensional physical system that shares most of the physics of a traditional sailing vessel, but also incorporates the complexity of the lifting surfaces producing forces in the Z-axis that raise the boat out of the free surface. The six degrees-of-freedom (DOF's) of the yacht are represented in the Fig. 2.3:

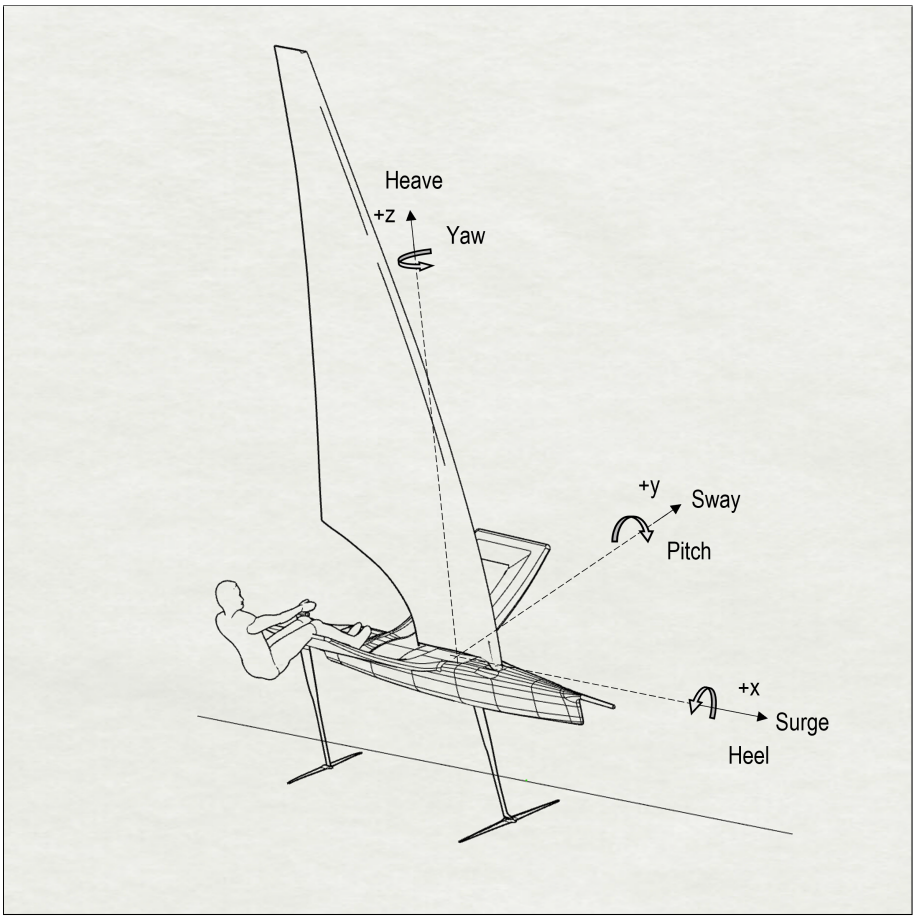


Figure 2.3: This figure shows the six degrees of freedom, one rotation and one translation per axis, of a sailing vessel, adapted to the geometry of an International Moth.

- Surge: the linear longitudinal motion along the $x$ axis.
- Sway: the linear transversal motion along the $y$axis.
- Heave: the linear vertical motion along the $z$ axis.
- Roll: the rotation longitudinal motion around the $x$ axis.
- Pitch: the rotation transversal motion around the $y$ axis.
- Yaw: the rotation motion around the $z$ axis.

The system represented in the Figure 2.3, has two main sailing equilibrium configurations: displacement and foiling, and the subsequent transition phase.

***Displacement Condition***

When speeds are low, the system mimics a traditional sailing boat. The equilibrium in Z is produced mainly by the buoyancy forces acting upwards and counteracting the weight. The dynamic forces are smaller at these speeds, so the behaviour of the yacht is expected to mimic the behaviour of a traditional sailing yacht (Fig. 2.2), but excluding the righting moment generated by the weight of the bulb and the keel. This is not precisely true in the current moth designs.

The foiling moths built in recent years are explicitly designed for foiling, often lacking crucial aspects of traditional sailing vessels, such as sufficient stability. Slender, low-displacement hulls, e.g., come with significant performance gains in aerodynamic drag but lack the stability of the more traditional hulls. A similar thing happens with all of the other characteristic elements of a moth, like the rigid wings, the small high aspect ratio rudder or the longitudinal position of the rig. All contribute to the lack of stability and control at low speeds. In certain conditions, such as a fresh trailing breeze, these boats are almost impossible to sail in displacement mode without specific rig settings and become quite dangerous.

In general, moths are sailed almost flat when sailing downwind and with windward heel in upwind conditions, both in displacement and foiling modes, for more efficiency and control [13].

***Foiling Condition***

A general YZ force diagram of a sailing moth is presented in the Figure 2.4:

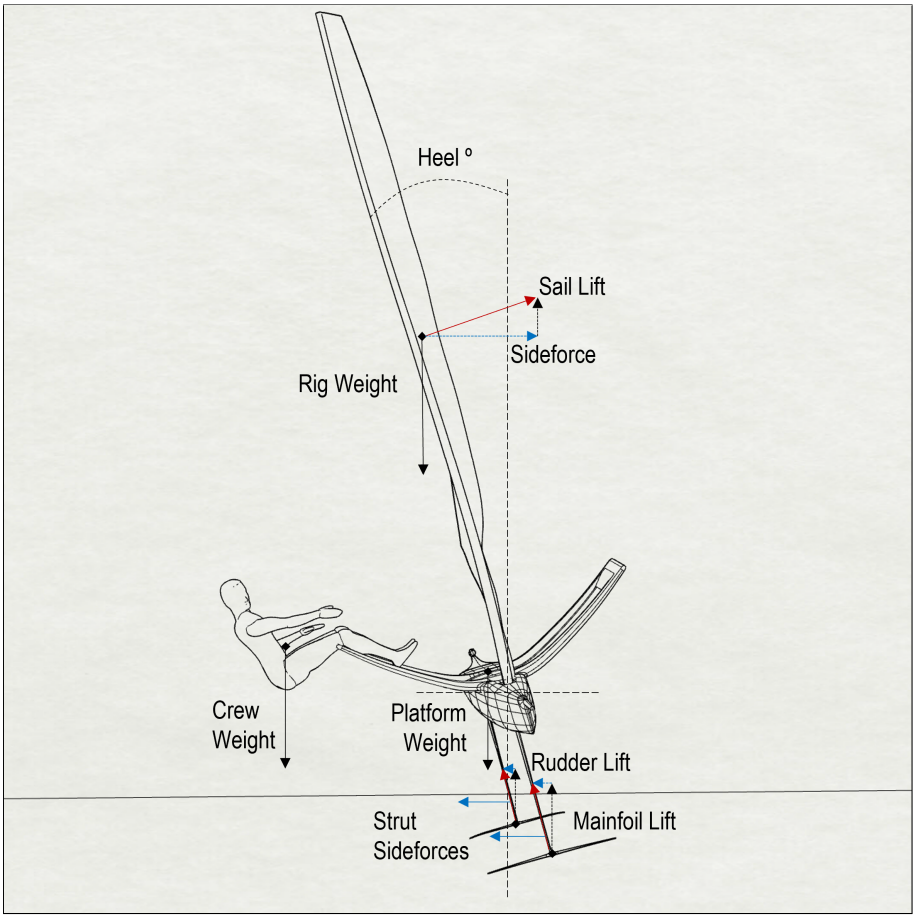


Figure 2.4: YZ equilibrium of the International Moth.

There are multiple benefits of sailing the moth with windward heel:

1. The righting arms between the crew, rig and hull weight and the foils' lifting force all increase.

2. The mainfoil wing increases its sideforce, counteracting the force generated by the sail (that decreases its y-force component and increases its z-component with heel, reducing appendage z-force requirements).

3. The reduction of the sail's driving force is a drawback that can be balanced by adjusting the sail profile (generally, in upwind conditions, a moth sail quickly needs de-powering, so inclining (canting) to windward the sailplan is not necessarily an adverse effect). In addition, the other benefits generally overcome the losses generated by sailing with windward heel in terms of VMG, and there are rigging solutions that enable rig canting.

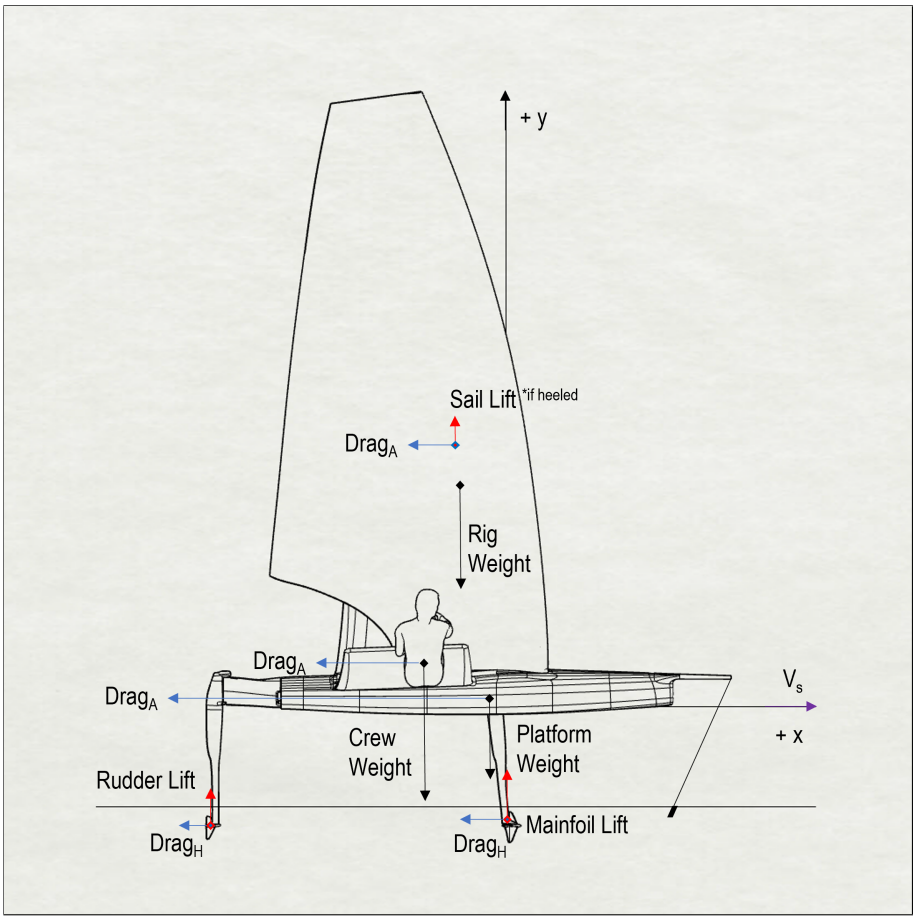


Figure 2.5: XZ equilibrium of the International Moth.

A general XZ force diagram of a sailing moth is presented in the Figure 2.5. The pitch of the boat is mainly controlled by changing the rudder force and the crew hiking position (in the latest moth designs, the longitudinal movement range has been significantly reduced due to the addition of smaller wings). Since the International Moth Class Rules do not contemplate the existence of a rudder elevator flap, the way of controlling the rudder force while foiling is by changing the rudder rake using a longitudinal screw connected to the tiller extension. The sailor can rotate the tiller extension to the left or to the right to increase or reduce the rudder rake angle.

## 2.3 The International Moth Class Rules

The International Moth is a single–handed *development* (open–rule) class: the rules are deliberately minimal so designers can pursue performance within a small set of dimensional and equipment constraints. In practice, the class defines a "box" for hull, beam, rig and sail, prescribes basic safety and identification requirements, and leaves most details (including hydrofoils and control linkages) open, provided they comply with the Racing Rules of Sailing as modified by the class [3].

### 2.3.1 Dimensional "box" and hull shape constraints

- **Overall hull length** (between perpendiculars, excluding removable stem/rudder fittings):

  $$\leq 3355, \text{mm}$$

  Attempts to increase effective waterline via fittings/fairings are prohibited, and minimum clearances between the hull and rudder fittings/fairings apply.[3]

- **Overall beam** (including hiking racks, which are part of the hull):

  $$\leq 2250, \text{mm}$$

- **Hollows and continuity**: no visible longitudinal air gap when viewed fore or aft; below the static waterplane, no local hollow $> 75$ mm in any section inside 2700 mm from the aft perpendicular; and any non-rudder foil must *protrude* from the hull below the static waterplane (i.e., no fully internal "daggerboard trunks" providing lift).[3]

- **Buoyancy**: at least two independent tanks/bags sufficient to float the boat plus 75 kg level when swamped, and with any one flooded still float the boat's weight + 10 kg.[3]

### 2.3.2 Rig and sail limitations

- **Mast length**: overall mast spars $\leq 6250$ mm. Any boom section or mast portion below 5185 mm from the mast top must pass through a 90 mm internal diameter ring (fittings excluded).

- **Sail plan**: the boat races with *one* sail; total measured rig area $\leq 8.25$ m$^2$ (mast area within the top 5185 mm is counted per the measurement manual). Luff–head geometry is limited by a 110° reference from the throat point. Wing sails are permitted *only* as single-element sections (no slots visible while sailing).[3]

### 2.3.3 Crew, hiking and prohibited equipment

- **Crew**: one person only. Righting moment may be transferred to the sail only via the hull/rigging/mainsheet system (hiking straps may be attached to the hull).
- **Prohibitions**: moving/detachable seats and *trapezes* are prohibited; multihull configurations are not allowed, nor sailing a permitted hull consistently as a multihull.[3]

Figure 2.6: Image of an International Moth (Maguire Exocet #4433) sailing in light winds, perfect for showing how the wand mechanism works. The wand touches the water and, through a linkage system (gearing and offset), it transmits a control input to the foil flap. Image Credit: Luis Sampedro Perez

### 2.3.4 Foils and appendages

The class leaves foil planform, sections and mechanisms broadly open, but within the hull box and continuity rules above. Definitions clarify that "*foils*" include any centreboard, fin or hydrofoil used for lift, stability or lateral resistance; the rudder is a steering device mounted to the hull/fittings; hiking racks are part of the hull. In modern practice, this leads to two T-foils (main T on the centreboard; T-rudder aft), but that arrangement is by convention, not mandate.

Key shape/installation constraints that affect appendage design are: (i) non-rudder foils must emerge from the hull below the static waterplane, (ii) fairings and fittings cannot be used to extend waterline length, and (iii) minimum stand-off for rudder fittings/fairings relative to the hull, except at structural connection zones, restricts ultra-tight fairing blends. These collectively shape gantry geometry, rudder stock spacing and main-foil case design.[3]

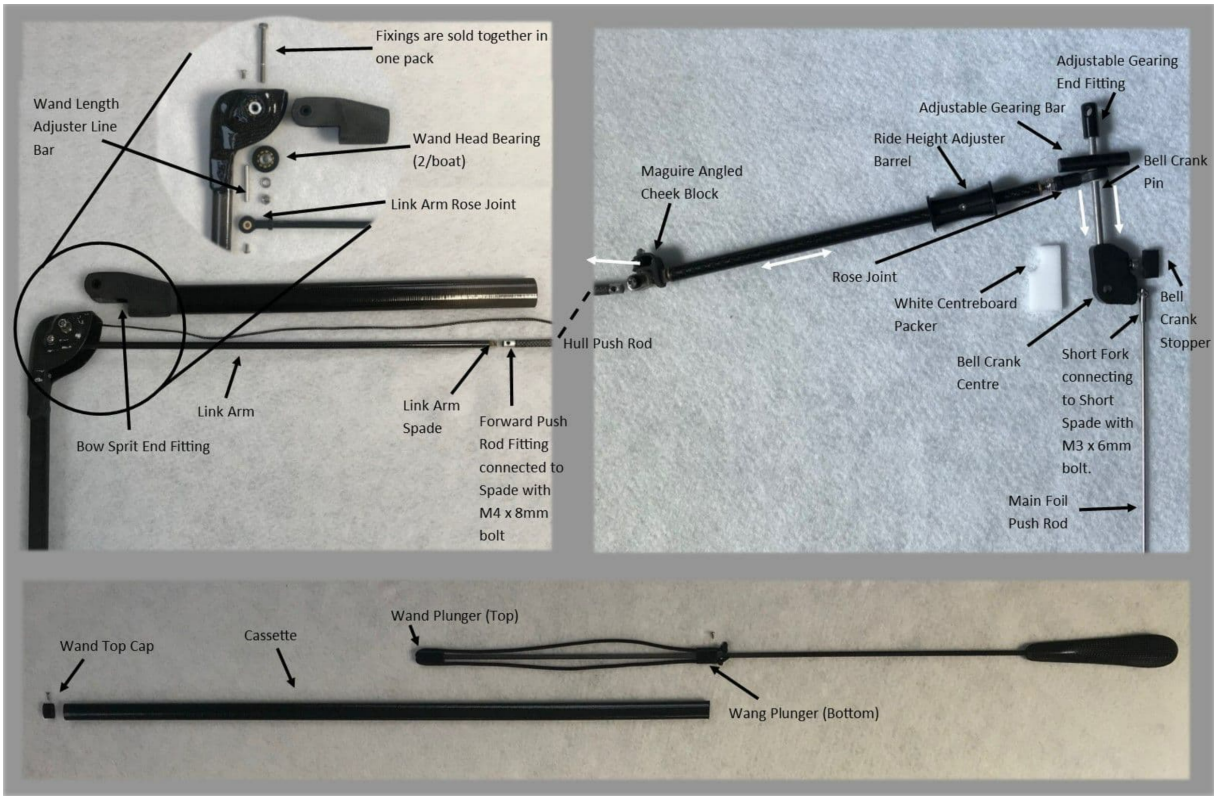


Figure 2.7: Main-foil linkage components for an International Moth (wand assembly, link arm, push-rods, bell crank and gearing, ride-height adjuster). Photograph adapted from Maguire Boats Online Shop, annotations by the author [14].

### 2.3.5 Flight-control systems

Two class modifications to the Racing Rules of Sailing are pivotal for the foiling dinghy:

1. **RRS 42 (propulsion) relaxation for take-off**: to initiate foiling, repeated/sudden body movements and multiple sheet pumps are expressly allowed. This allows common take-off techniques.

2. **RRS 52 (manual power) clarification**: only *remote controls using stored power* are prohibited; off-the-shelf small springs, shock-cord and similar are explicitly permitted in remote controls. In short, fully mechanical or hydro-mechanical linkages are fine; electrical/hydraulic/energy-storing actuation is not. It is clearly stated that electronic control systems are not permitted in the class, even though an electronic PID control system will be tested in this project.

Within those boundaries, modern Moths use a bow-mounted wand that senses ride height and drives the main-foil trailing-edge flap through a lever/push-rod/bell-crank system. Sailors can adjust ride height offset (neutral flap bias adjuster) and gearing ratio to tune lift with speed and sea state; wand length is also adjustable. Pitch is primarily trimmed by changing the T-rudder angle of attack via a helm-operated rake mechanism, which shifts the lift share between main and rudder foils. These mechanisms, shown in Figures 2.6 and 2.7 are fully mechanical and align with the prohibition of stored-power systems. The offset/gearing terminology follows established class usage [15] and is standard among sailors in the International Moth class (author's experience).

**Note on rudder devices.** The rules do not single out rudder flaps; in practice, pitch control is achieved by varying the whole-foil angle AoA ("rudder rake") rather than by a separate rudder–elevator flap.

## 2.4 Performance prediction

Predicting sailing speed has moved from steady equilibrium tools to fully dynamic, multi-degree-of-freedom models. The classic Velocity Prediction Program (VPP) solves a steady balance between aerodynamic drive and hydrodynamic resistance. It finds a state where forces and moments match, giving boat speed, heel and leeway for each true-wind condition, and then builds speed polars (Fig. 2.8 and optimal VMG angles. In practice, the VPP pulls its forces from empirical data, experiments, or lower-order numerical models of sails, hull and appendages, and an optimiser searches over trim and course to find the best steady solution. This framework remains the backbone for design work and rating systems [10], [16]–[18]. Beyond design work, VPPs are also used for handicap rules. The Offshore Racing Congress (ORC) has led public VPP development—from the IMS formulas to today's ORC VPP—and it publishes a clear force-model, updated regularly, to produce target polars and time allowances [10], [18], [19].

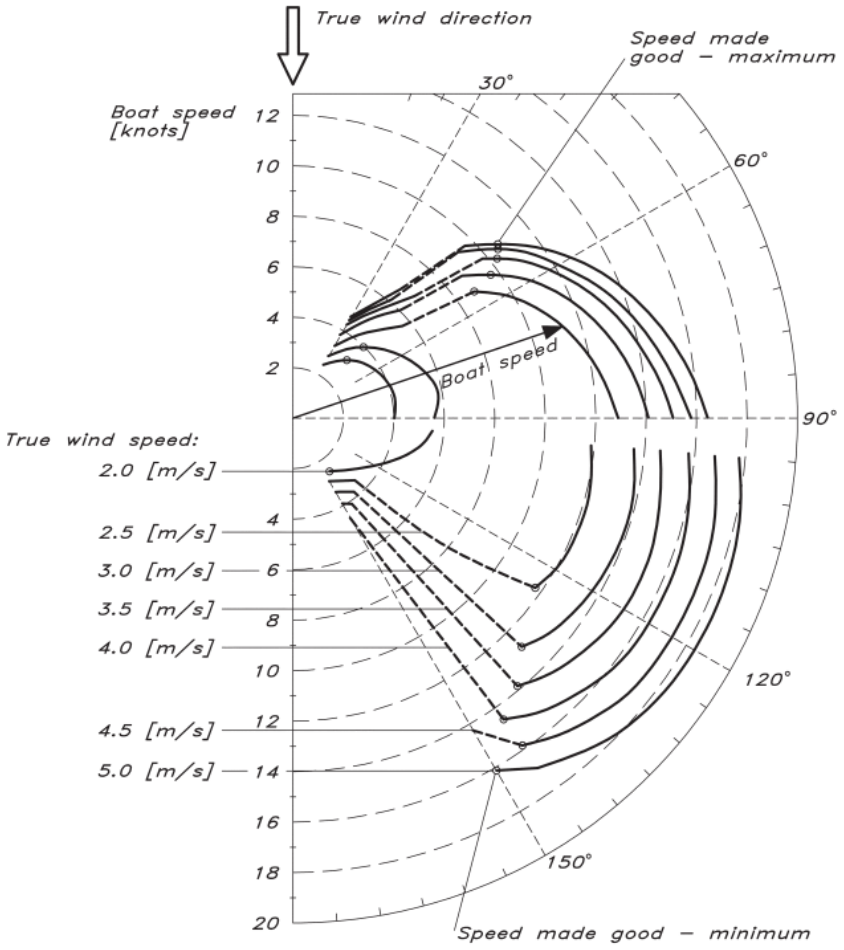


Figure 2.8: Example of a VPP polar plot. Each curve shows boat speed versus true-wind angle for a given true-wind speed; dashed semicircles indicate constant boat speed. Adapted from Eliasson & Larsson, *Principles of Yacht Design* (2022), Fig. 17.4 [10].

How a VPP "works" in simple terms is: choose a wind (speed and angle), assume a trial boat speed and attitude (heel, leeway), compute aero and hydro forces from the models, and iterate until surge, sway and roll moments balance within tolerance. The unknowns typically include boat speed, leeway angle, heel angle and some trim variables (e.g. sail trim or foil settings). The output is a steady state that represents how the boat would sail if the conditions were constant [10], [17].

For hydrofoilers, steady assumptions hide essential behaviour. Take-off, ride-height control and the strong coupling of heave–pitch–roll with foil AoA mean that performance depends on what happened a few seconds before and on the control inputs, not only on a single static point. Dynamic VPPs (DVPPs) address this by integrating the 6-DOF equations of motion in time, using a mix of runtime force models and precomputed datasets, and allowing unsteady wind, waves and mode changes between displacement and full flight. These tools show that you cannot trust steady polars alone to predict average speed or stability margins [20].

At the scale of the International Moth, early VPP studies already increased the number of freedoms and compared with field data (GPS and racing), showing that even compact models can capture the main trends when rig forces, foil aerodynamics and sailor mass placement are treated consistently [21]. Building on this, Eggert developed a Moth DVPP that couples flight mechanics, stability and control to the solver, so the model can find trimmed flying states and assess stability across the operating range [15].

Across larger foiling projects, the literature spans from quasi-static 6-DOF set-ups used for layout, rake/foil selection and polar generation, to time-domain DVPPs that capture time-to-flight, pitch–heave oscillations and controller effects. America's Cup work is a good example of this range and includes validations against race data [22]. In parallel, Castañeda shows how a time-domain VPP core can live inside a real-time simulator with autopilots and two-boat testing, useful for both design and training [1]. At the high-fidelity end, Persson's CFD-VPP combines a 6-DOF model with unsteady sail forces and waves to quantify where steady assumptions break down and how much accuracy you gain by going dynamic or CFD-coupled [23].

Finally, VPPs are now also used as optimisers. Adjoint-based methods can give gradients of VMG with respect to many foil shape variables and can handle multi-condition targets (upwind/downwind, several wind speeds), which is very relevant for foiling dinghies that operate across a wide envelope [24].

### 2.4.1 A state-of-the-art tool: The D3-VPP ®

The D3-VPP environment [25] was initially built around the FS-equilibrium VPP, but quickly became a state-of-the-art tool (Fig. 2.9). After more than 10 years of development, the D3-VPP has been used in projects like the Exploder Moth, the TF-35, the D3 A-Class catamarans, the Exploder F18, but especially in two four-year campaigns of America's Cup.

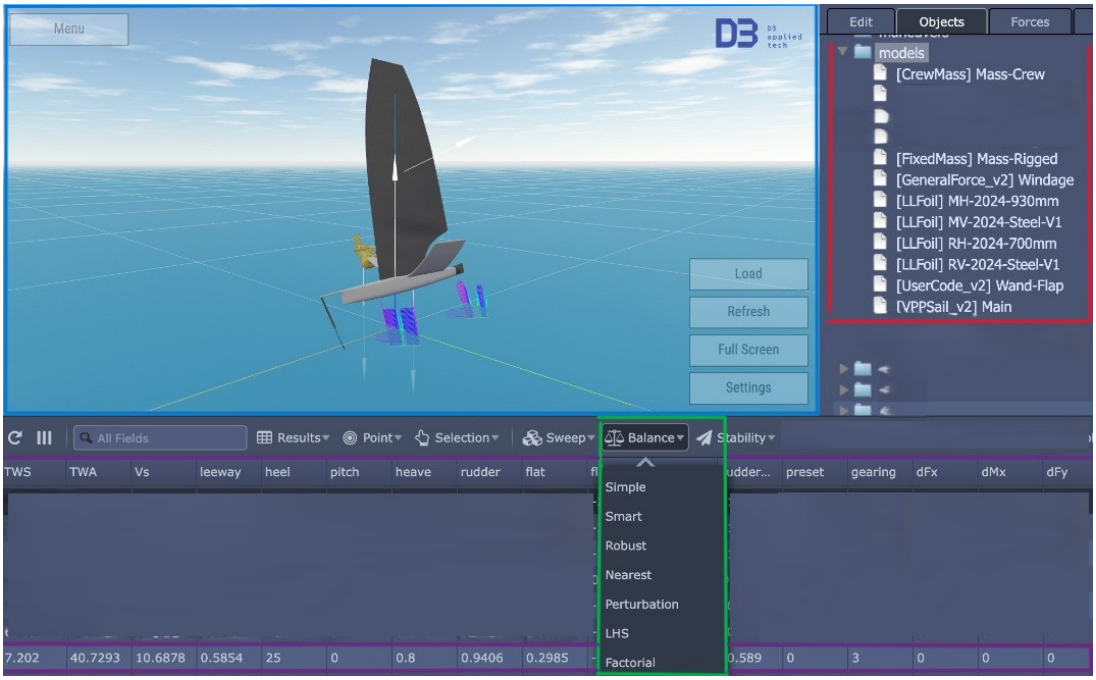


Figure 2.9: The D3-VPP tool features its own user interface, built on top of a complex optimisation routine designed to solve the equilibrium. In this figure the results and targets are highlighted in purple, the equilibium methods in green, the physics models in red and the geometry and lifting line forces in blue (top left).

The D3-VPP has the right-hand coordinate system located at the craft's centre of gravity, with the positive X direction pointing to the bow.

Inside the D3-VPP, the user enters the necessary geometry and the force models involved. The program has these models by default. Subsequently, the user selects the operating points around which they want to find the equilibrium. The program then solves the equilibrium using the chosen method. Finally, the user decides on alternative approaches to ensure the equilibrium point is correct.

It is necessary to import the geometry into the program in the form of a point cloud in `.csv` format. The point clouds of the hull, leading-edge points, and trailing-edge points of the mainfoil and rudder were imported in this case. Regarding the sail, the leading edge and the trailing edge of the sail, the area and the centre of area are included. All these points, areas and centres were taken from a Rhino 7 file containing the geometry.

***Force models***

The VPP force models that have been used are described below:

- **CFD Hull:** Advanced response surface model that allows specific flexibility for hull analysis. The model collects all the hydrodynamic forces that have previously been obtained with CFD analyses.
- **Crew Mass:** collects the weight of the crew and places it at the crew's centre of gravity, allowing for movement.
- **Fixed Mass:** places a fixed ballast at a point of the craft. In this case, it is used to take into account the Moth platform and rig weight.
- **General Buoyancy:** a model that collects the hydrostatic forces on the hull.
- **GeneralForce (Windage):** Response surface model that takes into account the windage obtained in CFD simulations of the platform, foils, wand and crew.
- **LL Foil:** Lifting Line model, developed by D3, that interprets the forces produced by the appendages (mainfoil and rudder verticals and horizontals), as a function of a series of parameters and coefficients and of the profiles of the geometry (more info in § 3.3).
- **CFD Sail:** Advanced response surface model, explicitly developed for the sails. As a function of a series of coefficients and of the geometry, it obtains the resultant force in the sails.

***Equilibrium***

To find the equilibrium sooner, heel and pitch are fixed in each of the cases to the values that the professional sailors who work in collaboration with D3 have found optimal.

The program solves the equilibrium by iterating on the system of equations. At the beginning, it starts with a single degree of freedom, and little by little the user adds degrees of freedom and released variables.

For each TWA, the variables that will be released will be: boat speed, leeway, rudder angle, flap angle, heave, rudder rake, crew longitudinal position and flat.

First, it explores the design space and identifies promising regions, using different methods of design of experiments (DoE) as a structured way to sample the input space, like the latin hypercube sampling (LHS) or a full-factorial design. Then a series of optimisers are run to find a value that maximises VMG (objective function). From the simpler gradient descent (ascent) method to more complex ones, a value is found and double-checked to mitigate local minima (with non-stochastic or the perturbations method, e.g.).

The values obtained in the VPP, presented in 4, will serve as a guide to carry out the simulations in Chapter 5 of the project.

### 2.4.2 VPP Limitations

In general, a VPP is a steady-state tool, which means that it is designed to predict equilibrium boat speed and performance under given constant conditions of wind, sail trim and heel. While this makes it powerful for exploring a wide range of design variations efficiently, its simplifications also impose essential limitations. A VPP assumes steady flow, constant forces and a perfectly balanced state, which makes it unsuitable for capturing non-linear or transient phenomena that occur in real sailing.

One of the main limitations of a VPP is, therefore, its inability to represent dynamic behaviour. Accelerations, decelerations, boat responses during manoeuvres such as tacks or gybes, or the transient behaviour during a bearaway are not captured because the tool is not designed for that. These effects are central in high-performance classes such as the International Moth, where quick responses and stability margins are critical.

Related to this is the treatment of the environment. A VPP generally assumes flat water and uniform, steady wind. In reality, sailors face waves, gusts, lulls, and wind shifts, which modify the loads on the boat and the sailor's response. These unsteady environmental factors are often decisive in determining performance, but they cannot be studied in a traditional VPP framework.

Finally, VPPs struggle when the boat operates near its physical limits. For the Moth, this includes situations such as flying close to the free surface, sailing with too little immersed rudder, or experiencing excessive heel. These are highly non-linear conditions, where small changes in control inputs or environment produce disproportionately large effects on stability and performance. A steady-state equilibrium model is not capable of capturing these edge-case behaviours accurately.

It is precisely in these areas where a dynamic simulator demonstrates its actual value. By modelling time-dependent responses, environmental variability, and non-linear interactions, a simulator can reproduce situations that a VPP cannot capture. This makes it a powerful test bench for analysing scenarios at the performance limits of a foiling Moth, and shows clearly the complementarity between both approaches.

### 2.4.3 VPP to Simulation

Real-time simulation appears as a solution for a couple of situations that the VPP can not predict correctly, as discussed in the subsection 2.4.2, about the limitations of the VPP. A classic VPP tells you the balanced, best-trim state for a given wind; a simulator lets the boat "live" in time—accelerate, fall off foils, overshoot pitch, recover—and shows how control inputs and sea state shape those transients. That's precisely what we need for a foiling dinghy: take-off timing, ride-height control, and stability margins depend on history and on the wand–flap and rudder-rake actions, not just a single equilibrium.

The idea is not new in top-level campaigns. Early America's Cup work already combined VPP logic with time-domain race modelling: from quasi-steady tools used around the 26$^{\text{th}}$ Cup era to explicit 6-DOF simulators (e.g. Day et al. [26], Harris [27]) that stitched together aerodynamic and hydrodynamic models to integrate the equations of motion and compare against full-scale data [20]. In parallel, modular VPP frameworks (e.g. FS-Equilibrium, [24], [28]–[30]) were built to plug different force models and either solve the steady balance or integrate the boat dynamics. Those same frameworks were even driven in *real time* inside the Twisted-Flow Wind Tunnel so that trimmers could see speed and heel change instantly with trim—closing the loop between aero measurements and the hydrodynamic state needed to balance them [17], [18].

Castañeda (2018, [1]) generalised this into a complete simulator architecture with a time-domain VPP at the core (force models + 6-DOF integrator). He argued this isn't just a "fancy VPP", but a modular tool that supports four program areas: a design asset (try concepts early, run two-boat studies with one real boat), a safe test platform (probe limits, test deck gear independent of weather), a comms hub between sailors and designers, and a training/race-prep platform. He also documented the details that make foiling boats work in the time domain: suitable autopilots for flight control, model corrections for piercing foils, step-size, etc.[1].

At the Moth scale, this shift is already in use. Brito (2019) showed how *Gomboc* can act as a DVPP and a race simulator for an International Moth: build blocks for hull, foils and aero; integrate the 6-DOF states; and run virtual races or A/B foil comparisons. His internship report also highlights the practical reality: aero/weight models still drive accuracy, but the simulator gives fast, design-relevant feedback (e.g. speed deltas on a tight reach when you swap foil geometries) that you simply do not get from steady polars alone [31].

In short, VPPs and simulators are complementary. The VPP is perfect for sweeps, polars and quick trade-offs; the simulator adds the missing time dimension: take-off, ride-height control and manoeuvres. That's why modern Cup teams run both: use SVPP/DVPP for layout, foil/rake and polar generation, then exercise the design and the mechatronics in a driver-in-the-loop environment [2], [22].

As said by Joseph Ozanne (2025), Alinghi Red Bull Racing Team's simulator for the 37th AC (Fig. 2.10) seamlessly integrated design development, mechatronics testing, crew training, and virtual racing. That platform, built inside Simulator in Motion, established simulation not as an option, but as a mandatory path to engineering excellence [2].


Figure 2.10: Latest generation foiling yacht simulator designed for the 37$^{\text{th}}$ AC. Frame captured from the Simulator in Motion homepage video [32].

# 3.

# Methodology for Modelling, Control, and Simulation

This chapter presents the methodology and set-up used to build a working digital twin of the International Moth in Simulator in Motion (SiM). It first outlines the modelling inputs (geometry, sections, parameters) and the SiM architecture (§ 3.2, including the folder structure, data flow, and load order used to initialise a run. It then (§ 3.3) details the physics modules (foils via `LLFSIhydro`, hull buoyancy, mass/inertia, and the aerodynamic model) and the control layer (three proportional–integral–derivative controller loops), highlighting key assumptions, interfaces, and limitations.

## 3.1 Modelling the International Moth

The main geometry Rhino 7 file of the hull, gantry, foils and sail was kindly provided by D3 Applied Technologies, S.L. (D3) at the beginning of the project.

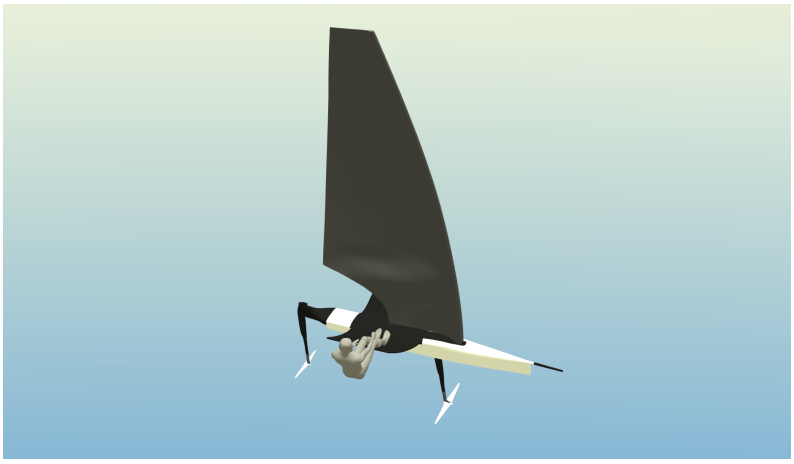

Figure 3.1: International Moth geometry modelled inside the Rhino 7 software

Fig. 3.1 shows all the parts of the 2025 Exploder MD3 v2 platform, including the foil set (one of the newest available from Exploder as of 2025) composed of the following parts:

- RV24 rudder blade + RE14 rudder elevator
- MV27 mainfoil vertical + MW18 mainfoil wing

(a)


(b)


Figure 3.2: (a) Exploder MD3 v2 International Moth crossing the finish line during the Moth Worlds 2025. Sailor: Diego Botin. Photo: Martina Orsini. [33]. (b) Screenshot of the International Moth completely assembled together, sailing inside the SiM environment built by the author

## 3.2 The Sailing Simulator: Simulator in Motion®

Simulator in Motion (SiM) is a company that develops high-end performance simulators for professional sailing teams and marine industries [2]. Their simulator (Fig. 2.10) is capable of running real-time physics models, solving force equilibrium, and applying those forces directly to the yacht's geometry, providing a highly realistic virtual sailing environment.

In this chapter, the functioning of SiM and the way its main components are structured will be described. Particular attention is given to the integration work carried out to connect the simulator with the D3-VPP physics model, enabling the creation of a working digital twin of the International Moth.

The simulator architecture is divided into several modules. The two central elements are the `SiM_Data` and `SiM_YachtManager` folders, complemented by a customizable Yacht folder. While the core simulator files function as a "black box" that cannot be directly modified by the student, the Yacht folder provides user-level access for defining geometry, parameters, physics and configuration.

Overall, SiM follows a modular design philosophy: each subsystem is encapsulated within its own directory, containing the necessary data, configuration scripts, and geometry files. This modularity ensures flexibility, scalability, and the possibility of coupling external models without interfering with the core simulator engine made with Unity.

Unity provides the runtime environment, the physics loop, and the rendering system. Unity executes the compiled `C#` scripts and manages the continuous update cycle required for real-time simulations. The simulator is launched as a standalone Unity application (`SiM.exe`), which integrates the physics solvers, the graphical interface, and the modular data subsystems into a single platform.

### 3.2.1 SiM_Data

The `SiM_Data` directory contains Unity-managed assets, configuration files, and subsystems (e.g., `globalgamemanagers`, `resources.assets`, `StreamingAssets`) that control the loading of parameters, resource bundles, and scenes at runtime.

### 3.2.2 Yacht Manager

In parallel, the `SiM_YachtManager` directory includes dynamic libraries (.dll and .so files) implementing specialised solver functions, such as hydrodynamic models (libwaves.so), control logics, and fitting tools. This separation ensures that the simulator operates as a closed "black box" where the proprietary physics modules remain protected, while user interaction is restricted to the Yacht folder.

The yacht manager is in charge of loading and managing the yacht folder and initialising the simulation.

### 3.2.3 SiM workflow

This is the order in which the yacht manager opens the different folders and initialises the solution. All these folders are mentioned in § 3.2.4, § 3.2.5.

The simulator starts only with the runtime and platform settings, first reading the global Unity configuration from INPUTS/COMMON (`unity_settings.xml`) and the ambient/oscillation definitions for the environment. It then includes the selected craft by loading the yacht model package, (MOTH (§ 3.2.5), in this case), pulling in the core yacht definition, variable set, initial conditions and model-level settings in that order (`yacht.xml,VARS/variables.xml,INIT/init_conditions.xml,SETTINGS/settings.xml`).

This is before any physics systems are initialised. The simulator is based on modules or blocks that are pre-defined inside the Simulator in Motion source code or defined by the user in the INPUTS folder (§ 3.2.5).

With the platform and yacht context set, the simulator proceeds one-by-one through the physics stack and then the control layer. It begins with the hull/float model and its baseline hydro tables, then configures appendages: the rudder module (XML) and its referenced polar tables, lifting-line data and rudder geometries; and the main foil module with its lifting-line polars and foil geometries. Next it loads the aerodynamic package (`sail.xml` plus off-range data, planform and textures/wing-shape tables), followed by auxiliary loads such as windage, mass (hull and crew) and instrumentation markers. Finally, the systems and logic layer is loaded (`systems.xml,logics.xml`, and its lookup tables) after which feature switches are read to enable/disable behaviours for the run. This ordered sequence guarantees that each module finds its dependencies.

### 3.2.4 Yacht Model

This folder, accessible by the user, provides the interface for defining geometry, parameters, and configuration files, allowing experimentation and debugging without altering the core simulation engine. This folder contains two subfolders: OUTPUTS and INPUTS.

#### *OUTPUTS*

The OUTPUTS folder includes 7 different files that are generated with each simulation, and that are really important for debugging and posterior analysis. The first is:

- `output_date_time.csv`

  This .csv file contains all the values that the variables take during the simulation and stores it in rows and columns. This file is the main source of information together with the visual interface. A `outputs-visualizer.html` file was created

during the project in order to plot and graphically see better the variables during the simulation runs and different tests.

And the other 6, are .list files that contain all the frames of reference, loaded files, switches, variables and units loaded in each simulation and their details, useful for contrasting information, debugging and double checking that everything is running correctly:

- `frames.list`
- `loaded_files.list`
- `loaded_files_info.list`
- `switches.list`
- `units.list`
- `variables.list`

***INPUTS***

The INPUTS directory contains all the data necessary to initialise and configure the simulation. The Inputs folder is structured in 4 subfolders and two .xml files:

- COMMON

  Shared inputs, accessible by all the models, and in case of multiple boat types, including:

  - Polars Here all the polars .csv files are stored for all the 2D profiles used in the appendages models. More info about these polars in § 3.3.1.
  - `unity_settings.xml` Important xml file that contains all the necessary settings for initialising a custom simulation, including available logic variables for different bindings, default cameras, etc.

- ENVIRONMENT

  Contains all the files in charge of defining and visualizing the environmental conditions, like the sea state (`seastate.xml`), the oscillations of the wind ( `oscillations.xml` ) and other options for two yacht testing like the wind shadow definition. During the tests made in 4 and 5 all these files were omitted, as the initial conditions were defined with another method, in `input_Moth.xml`.

- RACECOURSE

  This folder only contains the `racecourse.xml` file, needed in case there is a racecourse set for testing.

- `config.xml`

  This is a important .xml file that contains global settings like the refresh rate , the interpolation back time or the frequency of the outputs. It also defines the IPs and ports for the communication with the main server.

- `input_Moth.xml`

  Main input file that defines where the `yacht.xml` and `unity_settings.xml` files are. But also is used to the define the initial values of global environment variables like the air properties like density or pressure, initial TWS, TWD, and oscillations (defined in the `ENVIRONMENT/oscillations.xml` file), that are disabled as default.

  Also here the water properties like density, temperature and viscosity are defined. With options to define the sea current and sea state. Note that in this file is where the Wave01 (5.2) is created, with height 0.1 m, direction 220 deg and period 5.0 s.

- MOTH (See § 3.2.5)

### 3.2.5 INPUTS/MOTH Folder

Is a subfolder inside inputs. These is where the yacht model is defined and the parameters and geometry specific to the International Moth class are included, as well as the physics models. This folder includes the following folders (explained in depth below) and the `yacht.xml` file:

- SETTINGS
- PHYSICS
- VARS
- LOGICS
- SYSTEMS
- SWITCHES
- INIT
- `yacht.xml`

  This file, defines the name of the yacht and creates by default the Boat Frame of reference "BoatFrame". It also gives the relative paths to all the important files inside the MOTH folder. All the physics blocks are referenced here, but also the systems, switches, interface, scenario, initial conditions, settings, variables, logics, targets and markers files. These generally need a placeholder in case there are not referenced, because the yacht manager expects these files.

***MOTH/SETTINGS folder***

Includes the `settings.xml` file that defines the dynamic settings (time-step, solver, and inertial behaviour corrections), the simulator operational limits (maximum and minimum for state variables) and the unity settings (names for the geometry and blocks, all the monitoring variables available in real-time in the GUI and default cameras) of the yacht.

***MOTH/PHYSICS folder***

Equations and geometric data for hydrodynamic and aerodynamic modelling. Each folder corresponds with a physics model and a block of the simulator:

- PHYSICS/FOIL

  The FOIL folder contains the geometry points of the mainfoil vertical and horizontal, and also the `foil_moth.xml` file.

This file defines a LLFSIhydro (See § 3.3.1) model, with its corresponding "FoilFrame" as frame of reference. This frame of reference is located at the intersection of the leading edge of the strut with the hull, and all the geometry and variables inside this FOIL block are defined relative to this origin.

In the same file, the point of reference for flow measurement is defined in the intersection of the wing with the LE of the vertical, and the variable `foil_flap` is connected to the foil.

Finally, the definition of this appendage is done following the process described below:

1. The strut and wing polars are loaded as .csv files, and assigned a index number.
2. The geometry of the vertical and horizontal is loaded as points, and divided in segments in function of the different sections, with the purpose of executing the lifting-line theory.
3. The lifting-line theory settings are defined as in § 3.3.1.

- PHYSICS/HULL

  The HULL folder includes the `float.xml` file and the referenced files (the .stl geometry of the hull) and the dynamic forces-and-moments matrix in .csv. The xml file defines a hull_buoyancy physics model (see § 3.3.2) with its corresponding reference data and dynamic forces.

- PHYSICS/MASS

  Distribution of hull and crew masses models (See § 3.3.3) and frames of reference contained inside the .xml files: `hull_mass.xmlandcrew_mass.xml`.

- PHYSICS/RUDDER

  Almost mirroring the FOIL folder, the RUDDER folder contains the geometry points of the rudder vertical and horizontal, and also the `rudder_moth.xml` file.

  This file defines a LLFSIhydro (See § 3.3.1) model, with its corresponding "RudderFrame" as frame of reference. This frame of reference is located at the lower connection (gudgeon) of the leading edge of the blade with the gantry, and all the geometry and variables inside this RUDDER block are defined relative to this origin.

  In the same file, the point of reference for flow measurement is defined in the intersection of the elevator with the LE of the vertical.

  Finally, the definition of this appendage is done following the process described below:

1. The blade and elevator polars are loaded as .csv files, and assigned a index number.
2. The geometry of the vertical and horizontal is loaded as points, and divided in segments in function of the different sections, with the purpose of executing the lifting-line theory.
3. The lifting line settings are defined as in § 3.3.1.

- PHYSICS/SAIL

  This folder contains the `Moth_aero.xml` file and all the support files needed for the aero physics model (see § 3.3.4) to work properly. These include geometry, shape and texture files, off-range data and response surface files.

- PHYSICS/WINDAGE

  This folder contains all the different windage physics models, both with data from CFD (`windage_moth_LS.xml`) and simplified models (`windage_simple_zero.xml`), used to compute aerodynamic drag on non-lifting surfaces.

- `markers.xml`

  This file contains all the position markers and where they are defined. Here, z-coordinates of points like `markers.foil_imm`, `markers.rudder_imm` or `markers.bowsprit-z` are extracted. These are going to be important variables when processing the SiM outputs in 5 or when declaring the autopilots in § 3.2.5.

#### *MOTH/VARS folder*

**Note:** In SiM, each variable existing inside the inputs folder, starts with its folder tag followed by a dot (e.g. `environ.water.current.speed`, is a variable storing the speed of the `current` sub-block, defined inside the water sub-block of the environment block). All the variables inside the MOTH folder, start with "`yacht1.`" before its folder tag name if defined inside one of those folders, following recommended procedures from SiM (so that makes, e.g., `yacht1.RUDDER.boatWaterF_x` the resulting force of the rudder LLFSIhydro block projected in the x-axis of the boatWater reference frame).

Inside the MOTH/VARS folder is the file `variables.xml`. In this file, 6-types of simulation variables are declared. These variables are not defined by default by the SiM blocks, but instead are variables created by the user to be able to define logic controls or systems. The variables are englobed in one of those 6 types:

1. Parameters

   Affect directly the model, e.g., `parameters.rudder_rake` is a numeric variable that serves as value for the y-axis rotation of the RudderFrame in the RUDDER block.

2. Command

   The variable is commanded or receives an input from the keyboard or other gadgets, e.g., `command.rudder_rake` is a numeric variable that through a logic binding assigns the input of the keyboard to the variable `parameters.rudder_rake`.

3. Auto

   Similar to the command variables, these variables store inputs generated by the autopilots and can be connected to parameters through logic definitions.

4. Logic Vars

   Auxiliary variables for logics systems definition, normally boolean or numeric.

5. Target Vars

   Serve as target parameters for the autopilots, store numeric values.

6. Norm

   Store numeric values from previously normalized variables in the `logics.xml` file.

***MOTH/LOGICS folder***

The LOGICS folder includes the `logics.xml` file and all the files mentioned inside that xml. For this project the following internal systems were defined inside the logics module:

- Rate of Change module for the `command.rudder` variable, used when controlling manually the rudder angle (and thus the boat heading) using a keyboard, so it follows a controlled change of value when pressing the key.
- Step Change modules for the following variables:
  - `target_vars.twa`, to control the heading of the Yaw PID (§ 3.2.5) with the keyboard.
  - `target_vars.foil_imm`, to control the flight height of the Heave PID (§ 3.2.5) with the keyboard.
  - `target_vars.heel`, to control the target heel of the Roll PID (§ 3.2.5) with the keyboard.
  - `command.rudder_rake`, controls the amount of rudder rake changed with each keystroke.
  - `command.gearing`, idem for the gearing.
  - `command.RHoffset`, idem for the wand flight system offset variable.
  - `command.wand_length`, idem for the wand length parameter.

- Go to Target modules for this last 4 command variables mentioned, so the link is established with the parameter variable with the same name.
- Lookup table modules for the wand system (wand angle, gearing, see § 5.1) and for the twist in the Aero block (see § 3.3.4).
- Normalized value modules for variables like the TWA that is always positive.

***MOTH/SYSTEMS folder***

In the `systems.xml` file contained inside this folder are defined the 3 autopilots developed during this project, all three using the existing SiM `basic-PID` module:

- PID-Heave

  Changes `auto.foil_flap` to try and achieve the `target_vars.foil_imm` value in the variable `markers.foil_imm.position.z` (§ 3.2.5). Kp , Ki and Kd parameters are assigned, but also a multiplier, a rate (up and down) and the integral wind-up type.

- PID-Yaw

  Changes `auto.rudder` to try and achieve the `target_vars.twa` value in the variable `state.TWA`. Kp, Ki and Kd parameters are assigned, but also a multiplier, a rate (up and down) and the integral wind-up type.

- PID-Roll

  Changes `auto.flat` (§ 3.3.4) to try and achieve the `target_vars.heel` value in the variable `state.HEEL`. Kp, Ki and Kd parameters are assigned, but also a multiplier, a rate (up and down) and the integral wind-up type.

***MOTH/SWITCHES folder***

This folder includes the file `switches.xml` that uses the autopilot on/off state to switch between the variables that control the parameters.

***MOTH/INIT folder***

This folder contains the `init_conditions.xml` file, that defines the intial values of the most important parameters, targets and state variables before starting the simulation.

## 3.3 On Detail: Moth Physics Models

This section describes in detail the physics models that govern the main modules of the Moth within Simulator in Motion (SiM). The geometry definitions and foil sections were kindly provided by D3 Applied Technologies, S.L. (D3). Most of these inputs are documented here to ensure reproducibility; however, certain proprietary elements (like the foil sections) cannot be disclosed in full in this report.

### 3.3.1 Underwater Lifting Surfaces

The underwater lifting surfaces in the simulator are computed with `LLFSIhydro`, a lifting-line theory / vortex lattice method hybrid. Conceptually, it uses a Weissinger–L vortex-lattice discretisation: the wing is split into spanwise strips (Fig. 3.3, each represented by a single horseshoe vortex placed on the quarter-chord. This method accounts for sweep and twist. Section aerodynamics (including viscous effects, camber and flap influence) are not solved on the go; instead, they are supplied through precomputed 2D polars (lift, drag and moment) and blended spanwise according to the local section assignment. In the present setup, the solver reads $C_L$ and $C_m$ directly from the polars and uses a thin-airfoil slope for the geometric angle build-up. Viscous drag is enabled, while additional free-surface penalties are disabled. A symmetry factor is applied to mirror the foil effects. Buoyancy on submerged foil volumes is included.

(a)

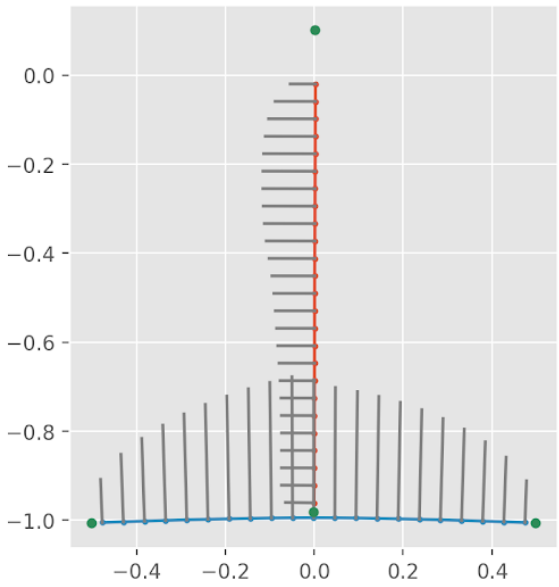


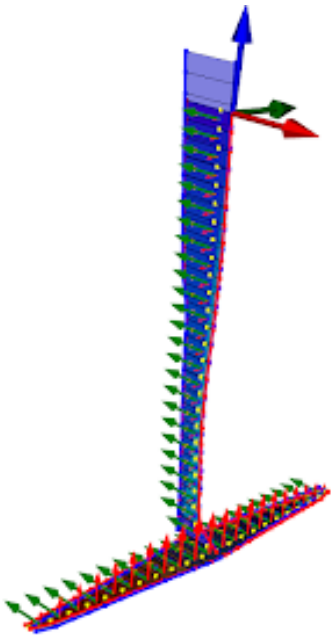

(b)

Figure 3.3: (a) planform discretisation and lift scheme for the main foil (Weissinger–L method). (b) 3D view of bound vortices and integrated loads for the mainfoil system.

***Main foil (MV27 + MW18)***

The main assembly is instantiated as `LLFSIhydro name="FOIL"` in the simulator frame and attached to `FoilFrame` at $\mathbf{r} = (-0.0267,\ 0.0,\ -0.0591)\,\mathrm{m}$, the junction of the vertical leading edge (LE) with the hull. A reference point for the flow evaluation is provided (in the t-connection, between the vertical and horizontal) and the flap deflection is linked to the global parameter `parameters.foil_flap`.

Hydrodynamics are supplied by two polar families: (i) the vertical strut MV27 (polar index 4), and (ii) the horizontal main wing MW18 (polar indices 0–3, covering tip/root variants and intermediate stations). The geometry is split into two parts with their own meshes (`n_panels=35` each): `main_vertical` reads the geometry file and assigns a constant 12% thickness with $x_t/c = 0.32$ across $u \in [0, 1]$ using the MV27 polar set; `main_horizontal` reads the wing geometry file and blends section polars spanwise (the sections of the horizontal change with a thicker section in the middle).

Operationally, the solver assembles a spanwise vortex lattice over those two parts, solves for circulation, and integrates sectional forces and moments using the supplied $C_L(\alpha, \delta)$ and $C_m(\alpha, \delta)$ tables (where $\delta$ is flap angle), returning 6-DOF loads to the foil model.

***Rudder (RV24 + RE14)***

The rudder assembly is defined as `LLFSIhydro name="RUDDER"` attached to `RudderFrame` at $\mathbf{r} = (-2.410,\ 0.0,\ 0.0225)\,\mathrm{m}$, next to the lower gantry gudgeon. Two control inputs are wired directly into the reference transform: first, a rake rotation about the $y$-axis (`ref_rot_y` ← `parameters.rudder_rake`, and second a steer/angle input about the $z$-axis (`ref_rot_z` ← `parameters.rudder`). A local `ref_flow` point is also specified in the junction between blade and elevator.

Hydrodynamic data are split between the vertical blade RV24 (polar indices 0–3, covering multiple span stations S2–S10) and the horizontal elevator RE14 (indices 4–6, including symmetric/asymmetric variants and the bullet fairing). Geometry is likewise split into `rudder_blade` and `rudder_elevator`, each meshed with `n_panels=35` and assigned section polars[1] along the non-dimensional span coordinate $u$. As with the main foil, the solver integrates the sectional loads from the polars and uses the thin-airfoil slope for angle build-up.

[1] **Notes on polars:** The simulator uses precomputed 2D polars for each section family (MW18, MV27, RV24, RE14). In our workflow these polars are generated by running AoA and flap sweeps in a 2D code (e.g., XFOIL) and exporting $C_L$, $C_D$ and $C_m$ tables that the solver reads at runtime. Stall and large-AOA detached-flow modelling is intentionally out of scope here, so an important limitation is that the simulator is not tuned to predict post-stall behaviour.

### 3.3.2 Hull Buoyancy

The hull buoyancy of the Moth is provided by the `hull_buoyancy` module named `FLOAT`. It is attached to the `BoatFrame` via `FloatFrame` with zero offset and rotation, so all hydrostatic forces and moments are returned in the boat frame. The solver reads a closed triangulated surface of the hull (`H037.stl`) and, at each time step, computes the submerged volume and its centroid from the mesh–free–surface intersection. The resulting buoyant load follows Archimedes' law,

$$\mathbf{F}_b = \rho_{\mathrm{w}} g \, V_{\mathrm{disp}} \, \hat{\mathbf{z}}$$

where $V_{\mathrm{disp}}$ is obtained from the instantaneous immersion. Two wave–elevation inputs (`fwd_probe`, `aft_probe`) allow the module to sample the ambient free surface along the hull; in the absence of a wave field they default to zero, producing still-water hydrostatics. Vertical damping terms can be added to account for the heave resistance. A CFD response surface file is supplied to account for the dynamic forces.

### 3.3.3 Mass and inertia

The mass of the hull was calculated, together with the inertias. This was an extensive process, made quicker with the Rhino 7 geometry file. Rhino helped to locate centroids and area moments, and then the parallel axis theorem was used.

The rigid-body of the hull is represented in the simulator by a single mass element (`single_mass name="hull_mass"`) attached to `BoatFrame` with its own `CGFrame`. The body's centre of gravity is at $\mathbf{r}_{\mathrm{CG}} = (-0.6953,\ 0.0000,\ 0.5319)\,\mathrm{m}$ respect to the BoatFrame, so the inertia tensor is defined about that CG frame. The total mass is $m = 40.9\,\mathrm{kg}$ and the principal moments are $(I_{xx}, I_{yy}, I_{zz}) = (64.260,\ 91.971,\ 32.790)\,\mathrm{kg\,m^2}$ with zero products of inertia $(I_{xy}, I_{xz}, I_{yz}) = (0, 0, 0)$, indicating alignment of the CG axes with the principal axes. The solver integrates the rigid-body equations with gravity applied at the CG and external aero/hydro loads supplied by the other modules.

The crew mass is 85 kg and is located in the CG of a person in hiking position at the starboard side of the hull.

### 3.3.4 Aerodynamic Sail Model

The `aero_sim_2.0` module models the rig with a data-driven response surface that returns aerodynamic force components as a function of apparent wind angle, depowering (`flat`) and a non-dimensional twist control. These forces are then dimensionalised by the dynamic pressure–area factor $qS = \frac{1}{2}\rho_{\mathrm{air}} A_{\mathrm{ref}} \mathrm{AWS}^2$ and applied at the rig's centre of effort in the boat frame. In the present configuration (`config MN-1`), the reference area

is $A_{\text{ref}} = 8.25$ m$^2$ [3]. These model also account for offrange data, visual shape, movement and textures of the sail.

That response surface was originally made for another project of the SiM company, and takes as basis the sail of a Nacra 17 tested in a wind tunnel. The model is more complex and has been further developed by the company, but the original source of some of the data for the response surface is taken from (Graf et al., 2020) [34].

**Important Note on the Sail Model:** this response surface already takes into account the losses due to windage of the rig and platform, this contrasts with the D3 Sail Model that was going to be used in the first assemblies of the simulator platform. This will be discussed also in § 4.6.

***Limitations***

This surrogate was preferred over the native D3 sail model because the current SiM build does not yet support a monosail configuration. The adapted model gives reasonable trends but has known gaps for a Moth:

(i) only two scalar controls (`flat`, `twist`) are exposed, so effects of specific trims (luff tension, outhaul, Cunningham) are absorbed implicitly[2];

(ii) yaw-moment from the off-centre mainsail may be not accurate as the model derives from a catamaran in a two-sail configuration

(iii) single-sail interaction/efficiency corrections (main vs. main+jib) are not applicable;

(iv) behaviour outside the calibrated AWA range relies on the off-range table rather than physics-based extrapolation. These limitations are important and revisited when discussing outputs in § 4.6.

[2]This modelling technique that uses the variable flat as overall sail flattening coefficient is widely used in the industry and described in literature, and works well for performance prediction and analysis

# 4.

# Assessing that the SiM outputs are consistent with VPP targets

This chapter benchmarks the Simulator-in-Motion (SiM) outputs against targets from the D3 Velocity Prediction Program (D3-VPP) at two representative operating conditions (upwind and downwind at TWS = 14 kn). The objective is to examine the consistency of predicted forces, moments and performance indicators, and to check that the internal balances are physically possible within the tested envelope. The chapter does not constitute a formal validation against sea trials or full-scale measurements, nor does it attempt to tune the simulator to match the VPP. D3-VPP is adopted as a suitable reference because it has been calibrated with extensive real-boat data and has been used to guide three generations of International Moth designs by the company; therefore, agreement with D3-VPP is interpreted as evidence of credibility for the simulator in these conditions.

## 4.1 Reference models and data

This section summarises the models used by the VPP and by the simulator, and the inputs shared by both.

The D3 Velocity Prediction Program (D3-VPP), described in 2.4.1, serves as the reference. For the present work we use, to compute steady equilibrium, the same force models listed there: CFD-based hull resistance, hydrostatics, crew and fixed masses, windage response surfaces, the *LL Foil* model for appendages, and the CFD-based sail response surface. The outputs taken as targets are the equilibrium forces and moments, boat speed and VMG, and the associated key variables (leeway, rudder angle, flap, heave, rudder rake, crew position and flat). D3-VPP uses a right-handed body axis system at the craft's centre of gravity with $+X$ pointing forward, which is retained here.

The Simulator-in-Motion (SiM) is run with the same craft geometry and mass properties as in the VPP. Equivalent physics modules are enabled to reproduce the same load contributions (foils, hull, masses, all described in § 3.3). The only important different is the use of a different Aero model. The VPP uses a more complex - International Moth oriented - model, while the SiM adapts a more general model - able to achieve similar results - . Each case is initialised using the attitude of the boat reported by D3-VPP, the simulation is allowed to reach a steady condition, and time-averaged outputs are recorded.

Common inputs and assumptions are harmonised across both tools: identical geometry (imported from the Rhino-derived point sets), mass and inertia properties, sail plan and foil configuration, crew mass and nominal position, coordinate conventions (values from the VPP are translated inside the simulator to the SiM coordinate system) and units. Environmental conditions are those in Table 4.1 (TWS = 14 kn; one upwind and one downwind operating point), with flat water and standard air/water densities. These aligned inputs ensure that any differences observed come from the modelling approaches rather than from data inconsistencies.

## 4.2 Test matrix and operating conditions

Two operating points were selected from the D3-VPP solution (optimum VMG) at a TWS of 14 kn to represent the Exploder D3 Moth targets for upwind and downwind sailing. The simulator cases are initialised with the attitude and state variables provided by the VPP at these points (Table 4.1) and run under the same environmental conditions. The aim is to reproduce the VPP targets and examine consistency.

Table 4.1: Target points extracted from VPP at TWS = 14 kn.

| **Parameter** | **Units** | **Upwind** | **Downwind** |
|---|---|---|---|
| TWS | kn | 14.0 | 14.0 |
| TWS | m/s | 7.202 | 7.202 |
| TWA | deg | 40.7293 | 147.0865 |
| $V_s$ | kn | 20.78 | 26.87 |
| $V_s$ | m/s | 10.6878 | 13.8211 |
| Leeway | deg | 0.5854 | 1.0282 |
| Heel | deg | 25 | 14 |
| Pitch | deg | 0 | 0 |
| Heave | m | 0.8 | 0.8 |
| Rudder | deg | 0.9406 | -0.1629 |
| Flat | adim | 0.2985 | 0.7535 |
| Flap | deg | -1.2942 | -2.587 |
| xCrew | m | 0.1 | 0.1 |
| RudderRake | deg | -0.589 | -1.0606 |
| Preset | | 0 | 0 |
| Gearing | | 3 | 3 |
| dFx | | 0 | 0 |
| dMx | | 0 | 0 |
| dFy | | 0 | 0 |
| dFz | | 0 | 0 |
| dMy | | 0 | 0 |
| dMz | | 0 | 0 |
| Config | | main,up,85kg | main,dw,85kg |
| Converged | | VMG | VMG |
| Objective | | 1,1,1,1,1,1 | 1,1,1,1,1,1 |
| DOFs | | Vs,leeway,rudder,flap,heave,rudderRake,xCrew,flat | same |
| AWA | deg | 15.8705 | 25.2466 |
| AWS | deg | 16.7847 | 8.5937 |
| VMG | m/s | 8.0275 | 11.7356 |
| Vs | kt | 20.7772 | 26.8683 |
| VMG | kt | 15.6056 | 22.8141 |
| TWS | kt | 14.0008 | 14.0008 |
| RigRM | Nm | 1416 | 1255 |
| Foil_tip_930mm | m | -0.0565 | -0.2148 |
| Rudder_tip_700mm | m | -0.1147 | -0.2528 |
| MH-FX | N | -36.416 | -51.0682 |
| MH-FY | N | -378.961 | -226.7877 |
| MH-FZ | N | 869.0485 | 965.9528 |
| MV-FX | N | -8.1165 | -16.6056 |
| MV-FY | N | -33.3642 | -140.0884 |
| MV-FZ | N | 3.9461 | -11.4017 |
| RH-FX | N | -17.1371 | -28.0515 |
| RH-FY | N | -67.5932 | -29.0667 |
| RH-FZ | N | 177.422 | 147.5363 |
| RV-FX | N | -8.9158 | -15.9018 |
| RV-FY | N | -82.81 | -111.0714 |
| RV-FZ | N | -24.0285 | -9.6647 |
| Rudder immersion | mm | -232 | -305 |
| Foil immersion | mm | -231 | -304 |
| Foil windward midspan | $C_l$ | 0.2635 | 0.164 |
| Foil leeward midspan | $C_l$ | 0.2525 | 0.16 |
| Foil midspan | Re | 629115.7072 | 813551.377 |

## 4.3 Variables and metrics compared

This chapter compares (i) performance, (ii) attitude, (iii) control settings, (iv) hydrodynamic force components, and (v) equilibrium residuals between the simulator outputs and the D3-VPP targets at two operating points (upwind and downwind at TWS = 14 kn).

(i) Performance metrics are boat speed $V_s$ (reported in knots) and TWA/AWA (degrees).

(ii) Attitude metrics are heel, pitch, and ride height; the latter is proxied by the simulator's ride–height $z$ marker and compared with the VPP heave target.

(iii) Control settings are rudder angle, foil–flap, rudder–rake, and flat.

(iv) Hydrodynamic loads are compared as main–foil and rudder forces in body axes $(F_x, F_y, F_z)$, where VPP values are the sums of the horizontal+vertical appendage contributions (e.g. MH+MV for the main foil).

(v) Finally, overall force and moment residuals $(\sum F_x, \sum F_y, \sum F_z, \sum M_x, \sum M_y, \sum M_z)$ are quoted as a coherence check.

Errors are reported as absolute differences $\Delta = Y_{\mathrm{SiM}} - Y_{\mathrm{VPP}}$ and percentage differences $\Delta\% = 100\,\Delta/Y_{\mathrm{VPP}}$ where applicable.

Acceptance bands are stated a priori: $\pm 5\%$ for $V_s$, $\pm 2^\circ$ for angles, $\pm 0.1$ m for ride height, and $\pm 10$–$15\%$ for hydrodynamic force components.

## 4.4 Method

The simulator–VPP consistency check followed the workflow in Fig. 4.1. Two reference operating points (upwind and downwind at TWS = 14 kn; Table 4.1) are taken from D3-VPP, the simulator is run under the same conditions.

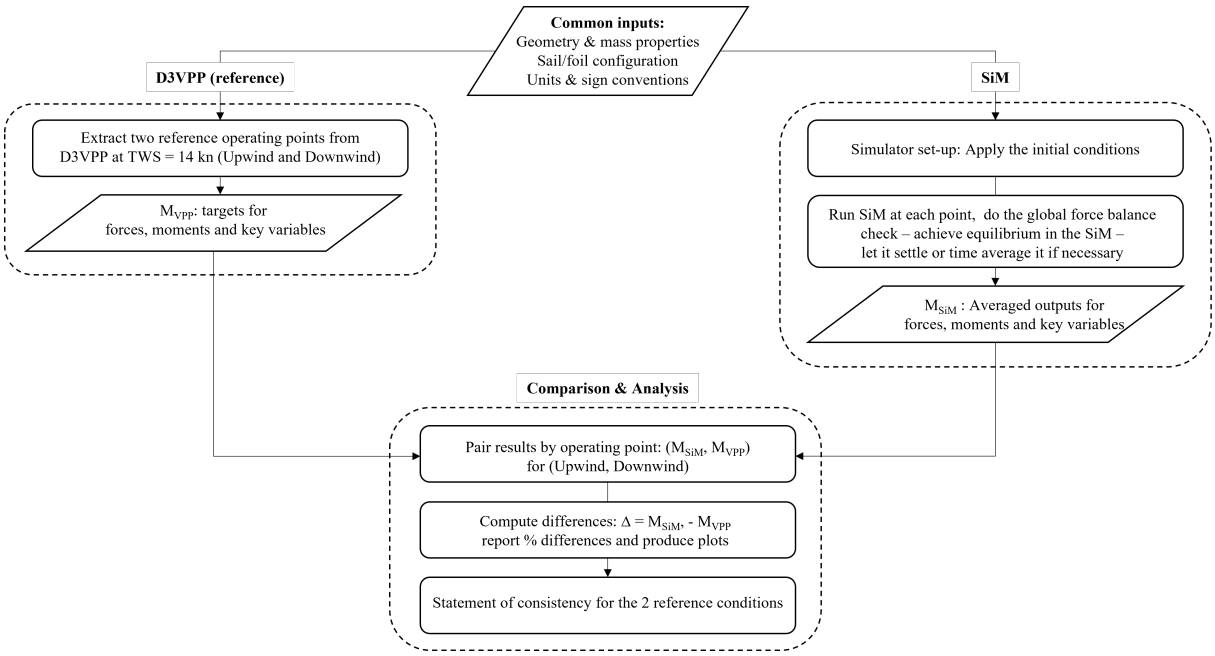


Figure 4.1: Workflow for simulator–VPP consistency checks at two reference points (upwind and downwind at TWS = 14 kn).

## 4.5 Results: agreement with VPP

### 4.5.1 Upwind Condition

On the upwind case (Table 4.2), $V_s$ is within +0.46% and VMG within +1.36% of the VPP target, with TWA and AWA essentially identical ($< 2°$ deviation in AWA). Heel matches the target exactly by construction, while pitch differs by +0.37°, which is small for this application. The foil immersion $z$ marker sits exactly in the VPP target. Hydrodynamic forces show good agreement on the main foil ($F_x$ and $F_z$ within ∼5%), with a modest deficit in side force ($F_y$) of 7.5% that is consistent with the lower leeway achieved by the simulator. The rudder lateral forces show the less accurate results, with discrepancies in the lateral force of the rudder, the rudder angle and the leeway. Force and moment residuals are numerically near zero.

Table 4.2: Upwind comparison at TWS = 14 kn; Simulator steady means vs D3-VPP targets (Sim, VPP, absolute and percentage differences). Note: % differences are relative to the VPP value. VPP main-foil forces are MH+MV; VPP rudder forces are RH+RV.

| **Group** | **Metric** | **Sim (mean)** | **VPP (target)** | **Δ (Sim–VPP)** | **Δ% vs VPP** |
|---|---|---|---|---|---|
| Performance | VMG [kn] | 15.818 | 15.606 | 0.212 | 1.36% |
| | $V_s$ [kn] | 20.873 | 20.777 | 0.096 | 0.461% |
| | TWA [deg] | 40.730 | 40.729 | 0.001 | 0.001% |
| | AWA [deg] | 16.181 | 15.871 | 0.311 | 1.954% |
| | Leeway (Landa) [deg] | 0.051 | 0.585 | -0.534 | -91.29% |
| Attitude | Heel [deg] | 25.000 | 25.000 | −0.000 | −0.000% |
| | Pitch [deg] | 0.370 | 0.000 | 0.370 | — |
| | Mainfoil immersion [m] | -0.231 | -0.231 | -0.000 | 0.04% |
| Controls | Rudder [deg] | 1.897 | 0.941 | 0.956 | 101.7% |
| | Foil flap [deg] | −2.180 | −1.294 | −0.886 | 68.45% |
| | Rudder rake [deg] | 0.589 | 0.589 | 0.00 | 0.00% |
| | Flat [adim] | 0.265 | 0.298 | −0.034 | −11.22% |
| Hydro forces | $F_x$ [N] | −45.093 | −44.533 | −0.561 | 1.26% |
| (FOIL) | $F_y$ [N] | −381.590 | −412.325 | 30.735 | −7.46% |
| | $F_z$ [N] | 831.792 | 872.995 | −41.203 | −4.72% |
| Hydro forces | $F_x$ [N] | −26.220 | −26.053 | −0.167 | 0.64% |
| (RUDDER) | $F_y$ [N] | −47.913 | −150.403 | 102.49 | −68.14% |
| | $F_z$ [N] | 236.100 | 153.394 | 82.706 | 53.9% |
| Equilibrium | $\Sigma F_x$ [N] | 0.043 | 0.000 | | |
| | $\Sigma F_y$ [N] | 0.005 | 0.000 | | |
| | $\Sigma F_z$ [N] | −0.002 | 0.000 | | |
| | $\Sigma M_x$ [N·m] | 0.001 | 0.000 | | |
| | $\Sigma M_y$ [N·m] | −0.000 | 0.000 | | |
| | $\Sigma M_z$ [N·m] | 0.000 | 0.000 | | |

### 4.5.2 Downwind Condition

In the downwind case (Table 4.3), the primary performance again matches closely: $V_s$ is within +0.34% and VMG within −0.72%, with TWA and AWA essentially on target (differences 0.07° and ∼1.3°, respectively). Heel is on target; the simulator settles with a small nose-down pitch (−2.15°), that shows again discrepancies in the rudder forces controlling MY and MZ. The simulated mainfoil immersion is within 0.011 m of the VPP target. The main-foil forces align to within ∼7–13% across axes. Totals ($\sum F, \sum M$) over the steady window are close to zero, indicating a clean steady equilibrium in the run.

Table 4.3: Downwind comparison at TWS = 14 kn: simulator steady means (new run) vs D3-VPP targets. Percentage deviations re relative to the VPP value. VPP main-foil forces are MH+MV; VPP rudder forces are RH+RV.

| **Group** | **Metric** | **Sim (mean)** | **VPP (target)** | **Δ (Sim–VPP)** | **Δ% vs VPP** |
|---|---|---|---|---|---|
| Performance | VMG [kn] | 22.650 | 22.814 | -0.164 | -0.719% |
| Performance | $V_s$ [kn] | 26.960 | 26.868 | 0.091 | 0.340% |
| Performance | TWA [deg] | 147.157 | 147.087 | 0.071 | 0.048% |
| Performance | AWA [deg] | 26.547 | 25.247 | 1.300 | 5.149% |
| Performance | Leeway (Landa) [deg] | 0.018 | 1.028 | -1.010 | -98.220% |
| Attitude | Heel [deg] | 13.996 | 14.000 | -0.004 | -0.032% |
| | Pitch [deg] | -2.149 | 0.000 | -2.149 | — |
| | Mainfoil immersion [m] | -0.315 | -0.304 | -0.011 | 3.720% |
| Controls | Rudder [deg] | 1.657 | -0.163 | 1.820 | -1 117% |
| | Foil flap [deg] | -0.116 | -2.587 | 2.471 | -95.511% |
| | Rudder rake [deg] | -1.061 | -1.061 | -0.000 | 0.000% |
| | Flat [adim] | 0.306 | 0.753 | -0.447 | -59.383% |
| Hydro forces | $F_x$ [N] | -73.821 | -67.674 | -6.147 | 9.083% |
| (FOIL) | $F_y$ [N] | -341.312 | -366.876 | 25.564 | -6.968% |
| | $F_z$ [N] | 1 075.256 | 954.551 | 120.705 | 12.645% |
| Hydro forces | $F_x$ [N] | -39.013 | -43.953 | 4.940 | -11.239% |
| (RUDDER) | $F_y$ [N] | -82.964 | -140.138 | 57.174 | -40.80% |
| | $F_z$ [N] | 88.950 | 137.872 | -48.922 | -35.484% |
| Coherence (totals) | $\Sigma F_x$ [N] | 0.972 | 0.000 | | |
| | $\Sigma F_y$ [N] | -0.010 | 0.000 | | |
| | $\Sigma F_z$ [N] | -4.286 | 0.000 | | |
| | $\Sigma M_x$ [N·m] | -4.637 | 0.000 | | |
| | $\Sigma M_y$ [N·m] | 4.049 | 0.000 | | |
| | $\Sigma M_z$ [N·m] | -0.465 | 0.000 | | |

## 4.6 Discussion

Overall, the simulator reproduces the D3-VPP targets credibly at both operating points, with small errors in the primary performance quantities and coherent internal balances. The largest differences across both points appear in (i) *control settings* and (ii) *lateral load partition*. In downwind, the simulator's steady rudder angle is about $+1.8°$ (VPP target $-0.16°$), and the foil flap is $\sim 2.5°$ less negative than the VPP trim. This reflects the different control logic: SiM reaches equilibrium via PID control, whereas the VPP constructs a steady trim that satisfies algebraic balance. Consequently, SiM can achieve the same performance and force levels with a different combination of controls. On lateral load, the simulator tends to carry slightly less leeway than the VPP (e.g. $0.02°$ vs $1.03°$ downwind), possibly implying a higher aerodynamic side force [1] and/or different lift distribution between main foil and rudder [2]; this is consistent with the observed differences in $F_y$ by appendage.

Taken together, these results support the intended use: within the tested envelope, SiM produces speeds, headings and force levels in line with an empirically calibrated VPP, while providing time-domain attitude and control histories that a steady solver cannot. Where non-negligible differences remain (e.g. pitch bias and downwind control variables), they are explainable by the differences between the models (and control systems) in the SiM and the VPP rather than by gross physics errors.

[1] The most probable explanation of these discrepances are the aero sideforces and moments generated by the aero model of the SiM. This is the only model that is not built around the corresponding VPP model.

[2] Less probable because the lifting-line theory models are really similar between SiM and VPP

## 4.7 Limitations and applicability

The comparison is deliberately narrow: two operating points at a single wind speed (TWS = 14 kn), in flat water, using a short steady window. No systematic sweep over TWS/TWA or sea states is attempted. The VPP is adopted as the reference based on its calibration against real-boat data; however, this is not a substitute for direct full-scale or towing-tank comparisons. In the simulator, the closed-loop controllers (wand/PID) and actuator limits are left as-is rather than tuned to "match" the VPP trims; this choice makes the comparison more representative of operational use, but it also explains differences in achieved control angles. Small residual risks remain around details of the aerodynamic model.

Accordingly, the results apply to the tested craft configuration (Exploder D3 Moth), mass properties and appendage set-up, within the vicinity of the two target points (upwind around $TWA \approx 41^\circ$ and downwind around $TWA \approx 147^\circ$ at 14 kn). In this sense, the simulator can be used with confidence for controller studies, sensitivity checks and qualitative design iteration. Extending applicability to broader conditions will require repeating the analysis over a matrix of TWS/TWA, waves, and different attitudes.

# 5.

# Developing a Flight Control System for the International Moth Simulator

The first flight control system developed was a PID controlling the mainfoil flap angle as a function of the moth's ride height (explained in-depth in § 3.2.5).

The second flight control system focuses on the mechanical parts, and replicates the boat's actual wand + pushrod connection, using the wand angle between the bowsprit and the free surface to output a flap angle, modified by a gearing mechanism.

A set of analyses were conducted to assess the sensitivity of the two flight control systems to different key variables, in flat water and excited by a regular wave of H = 0.1 m, in upwind and downwind conditions.

The influences of different variables are studied:

- Gearing (See § 5.3)
- Wand Length (See § 5.4)
- PID variables (Kp, Ki and Kd) (See § 5.5)

Section 5.1, below, explains how the wand mechanism was modelled. Section 5.2 gathers the initial conditions for all the tests and, finally, in § 5.6 the two systems are compared.

## 5.1 Experimental set-up

The strategy followed for designing the wand system in the simulator is divided into 5 stages:

- Stage 1. Gather the geometry of the Exploder D3 Moth wand mechanism and create a Rhino 7 plus Grasshopper environment.
- Stage 2. Using the gearing connections shown in Fig. 5.1, create a .csv table that links each gearing position (ranging from 1 to 6) to a flap angle. The results of this lookup table are shown in a more visual way in Fig. 5.2.
- Stage 3. Create a logic connection to the lookup table inside the simulator. This connection outputs a flap angle for each input combination of wand angle and gearing.

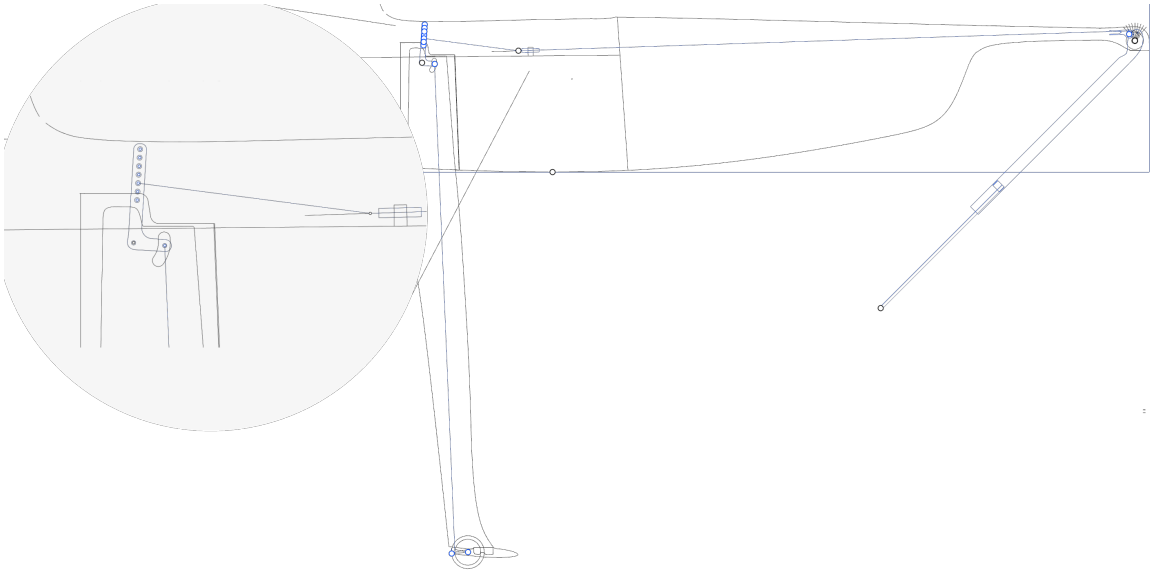

Figure 5.1: Gearing mechanism geometry file visualised in Rhino 7, courtesy of D3.

- Stage 4. Model, using Grasshopper, the attitude (geometry transforms of rotations and translations) of the Moth with a defined wand length and find (using a simple line search GH python code) the wand angle that makes the end of the wand touch the water. Then, export the lookup table. With the objective of making the calculation quick, it was decided to discretise the range and obtain 2025 combinations of equispaced points ranging from:
  - 0.7 to 1.2 for Wand Length (m) (5 values)
  - -30 to 30 for Heel (deg) (9 values)
  - -2 to 2 for Pitch (deg) (5 values)
  - -0.3 to 1.2 for Heave (m) (9 values)
- Stage 5. Create a second logic connection inside the SiM that interpolates a value of wand angle for each input combination of wand length, heel, pitch, pitch and heave given.

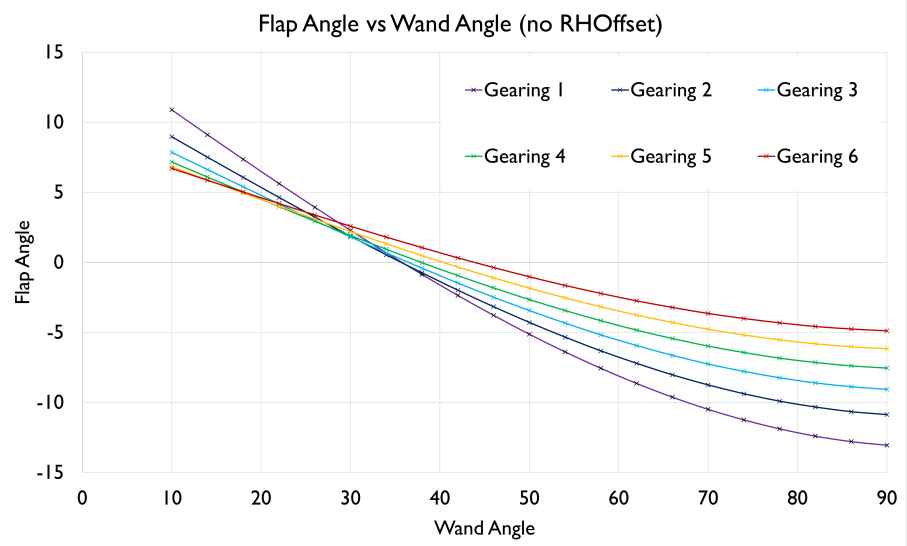


Figure 5.2: Gearing relation. For a determined wand angle a flap angle is given.

## 5.2 Initial Conditions

This initial conditions (§ 3.2.5) used to initialize the simulation have been extracted from the VPP results at a true wind speed (TWS) of 14 kn, corresponding to both the downwind and upwind performance points. This initial values are shown in Table 5.1 below:

Table 5.1: Initial platform testing points extracted from VPP at TWS = 14 kn.

| Variable | Unit | Upwind (14kn TWS) | Downwind (14kn TWS) |
|---|---|---|---|
| TWA | deg | 40.73 | 147.09 |
| Vs | kt | 20.78 | 26.87 |
| Heave | m | 0.7 | 0.7 |
| Heel | deg | 25 | 14 |
| Pitch | deg | 0 | 0 |
| Target TWA | deg | 40.73 | 147.09 |
| Target Heel | deg | 25 | 14 |
| Target Foil Imm. | m | -0.231 | -0.304 |
| Rudder rake | deg | 0.589 | -1.0606 |
| Rudder | deg | -0.9406 | -0.1629 |
| Foil Flap | deg | -1.2942 | -0.587 |
| Flat | adim | 0.2985 | 0.3535 |
| RH offset | deg | 30 | 30 |
| Wand Length | m | 1.00 | 1.00 |
| Gearing | adim | 3 | 3 |

### 5.2.1 Waves

To characterise the system response under waves in a controlled and repeatable way, we model the sea state with the simplest non-trivial excitation. Although the simulator can reproduce arbitrary irregular seas by superposing multiple wave trains, in this study we adopt a *single regular wave* so that differences across runs can be attributed to the parameter under test rather than to changes in the environment. This choice keeps the forcing well defined (known amplitude, direction and period) and makes the comparisons across upwind/downwind and flat/wave cases straightforward.

Each wave-condition run is simulated for at least 60 s to allow the transient to decay and the solution to reach a steady (often periodic) regime; for readability, figures report only the first 30 s. The wave used throughout the study—hereafter **Wave01**—is specified in Table 5.2: a regular head-sea wave with height $H = 0.10\,\mathrm{m}$, period $T = 5.0\,\mathrm{s}$, zero phase, and incidence angle $\beta = 0°$.

Table 5.2: Parameters of Wave01

| Wave name | Wave01 | |
|---|---|---|
| Wave Height | 0.1 | m |
| Angle | 0 | deg |
| Period | 5.0 | s |
| Phase | 0.0 | rad |

## 5.3 Gearing Sensitivity

The gearing ratio is a key control of the International Moth flight system. This parameter changes how the boat behaves in waves. Sailors adjust this control to determine whether the boat should follow the contour of every wave or maintain an average height to minimise wave effects. A side effect of the gearing when trimmed alone is a variation in ride height. Based on reports of professional sailors [35] and my own Moth sailing experience, we can say that less flap input per degree of wand angle generally reduces the lift produced by the mainfoil.

In this section, 24 simulations with changing gearings and environmental conditions were run (N = 24) and the resultant behaviour of the boat was analysed to describe the effect of the gearing on the ride height and boat performance.

Table 5.3: Details of the simulations performed in § 5.3

| Simulation ID# | Condition | Waves | Gearing |
|---|---|---|---|
| 1 | Upwind | Flat | 1 |
| 2 | Upwind | Flat | 2 |
| 3 | Upwind | Flat | 3 |
| 4 | Upwind | Flat | 4 |
| 5 | Upwind | Flat | 5 |
| 6 | Upwind | Flat | 6 |
| 7 | Upwind | Wave01 | 1 |
| 8 | Upwind | Wave01 | 2 |
| 9 | Upwind | Wave01 | 3 |
| 10 | Upwind | Wave01 | 4 |
| 11 | Upwind | Wave01 | 5 |
| 12 | Upwind | Wave01 | 6 |
| 13 | Downwind | Flat | 1 |
| 14 | Downwind | Flat | 2 |
| 15 | Downwind | Flat | 3 |
| 16 | Downwind | Flat | 4 |
| 17 | Downwind | Flat | 5 |
| 18 | Downwind | Flat | 6 |
| 19 | Downwind | Wave01 | 1 |
| 20 | Downwind | Wave01 | 2 |
| 21 | Downwind | Wave01 | 3 |
| 22 | Downwind | Wave01 | 4 |
| 23 | Downwind | Wave01 | 5 |
| 24 | Downwind | Wave01 | 6 |

### 5.3.1 Analysis

The simulations were made with the six different gearing configurations for a range on upwind and downwind conditions in flat water and subject to Wave01. The 24 runs and its key parameters are compiled in Table 5.3. All the results presented in the section § 5.3.2 below cover the first 30 seconds of the simulations, although the runs that include seastate were simulated at least for 60 seconds to ensure that the systems

The objective is to determine the response in z of the boat, to draw some conclusions about the effect of the gearing in the mechanical flight control system. The parameter

chosen to describe this response is the mainfoil immersion[1], as this is closely related to the mainfoil flap angle (manipulated variable).

### 5.3.2 Results

As an example of the simulator output, Fig. 5.3 shows the foil immersion with and without waves. The foil immersion curves illustrate the typical shape that the heave response adopts: (i) A first bump until the simulation equilibrium converges and then a horizontal line maintaining a stable flight in flat water - with a properly trimmed gearing. (ii) In waves, the boat is excited up and down following the wave, and stabilises around the equilibrium ride height oscillating periodically (in the case of ID-12, with a lower amplitude and period (0.04 m, 2 s) than the wave (0.5 m, 5 s), the latter due to the effects of the boat speed in the wave encounter frequency).

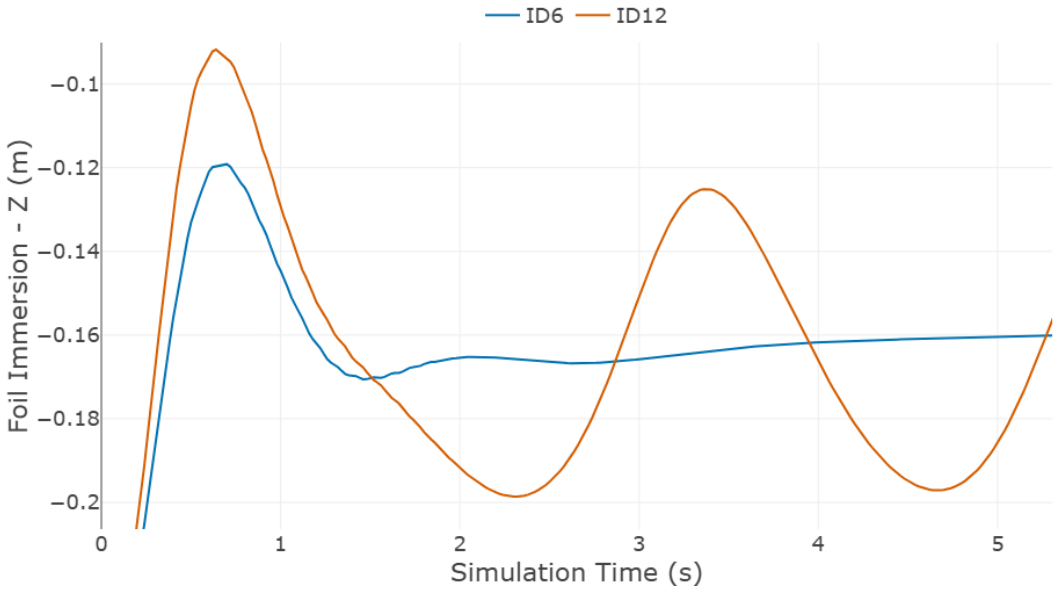


Figure 5.3: Foil immersion for upwind conditions in flat water versus wavy conditions. The figure shows the first 5 seconds of two different simulations, running with (orange line, ID-12) and without seastate (blue line, ID-6).

[1]The mainfoil immersion is measured as the t-junction marker position in z (See § 3.2.5)

***Upwind performance in flat water conditions***

Figure 5.4 compares six *mechanical* wand–flap gearings in upwind, flat-water runs. For the higher-response settings (ID1–ID5, i.e. larger flap change per degree of wand angle; see Fig. 5.2) the system settles into a sustained, near-periodic motion in foil immersion (Fig. 5.4a), which is mirrored in the VMG trace (Fig. 5.4b). This behaviour is consistent with an over-responsive linkage: small variations of wand angle lead to flap deflections that overcorrect the lift and feed back into ride height, likely reinforced by platform couplings (roll and target-TWA loops also oscillate in these runs). Reducing the gearing to ID6 lowers the effective loop gain and damps the mode: the boat reaches the target ride height promptly and maintains a steady flight, while VMG converges smoothly. Within the tested envelope, ID6 is the only gearing that delivers a stable operating point in flat water and is therefore the preferred baseline.

(a)

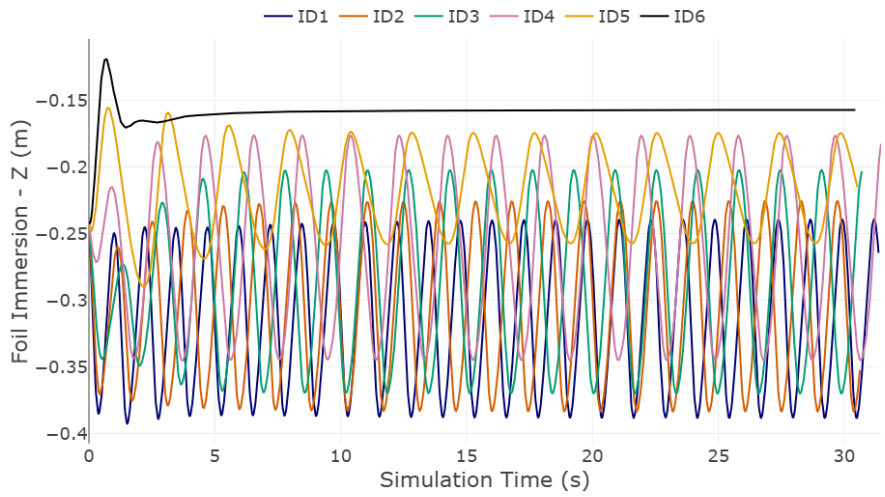


(b)

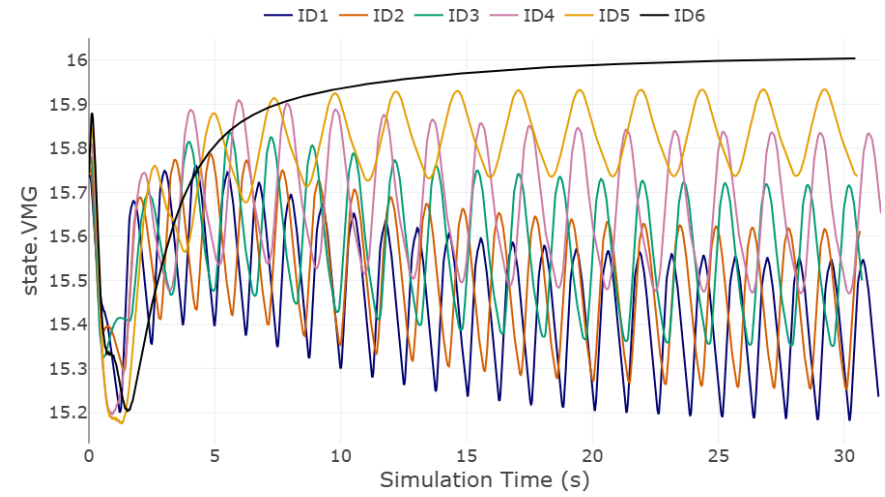


Figure 5.4: Sensitivity of the flight control system to changing gearing ratios in upwind sailing in flat waters conditions in terms of foil immersion (Fig. 5.4a) and upwind performance (VMG in kn; Fig. 5.4b). The six gearing ratios tested are shown, increasing progressively from greater ratios (ID1) to smaller response ratios (ID6) (see Table 5.3). First 30 seconds of each simulation are shown.

***Upwind performance under regular wave conditions***

Figure 5.5 extends the analysis to runs with Wave01. The response is driven primarily by the wave–encounter frequency: foil immersion oscillates about the ride height (Fig. 5.5a) and VMG exhibits the same modulation (Fig. 5.5b). The gearing mainly sets the effective loop gain of the mechanical linkage. Higher-response settings (ID7–ID11) track the wave more tightly and produce larger oscillation amplitude in both $z$ and VMG, whereas the lowest-response setting (ID12) attenuates the motion and yields the smoothest VMG growth. Within the tested range, reducing the gearing improves ride-height stability against waves without penalising the mean performance.

(a)

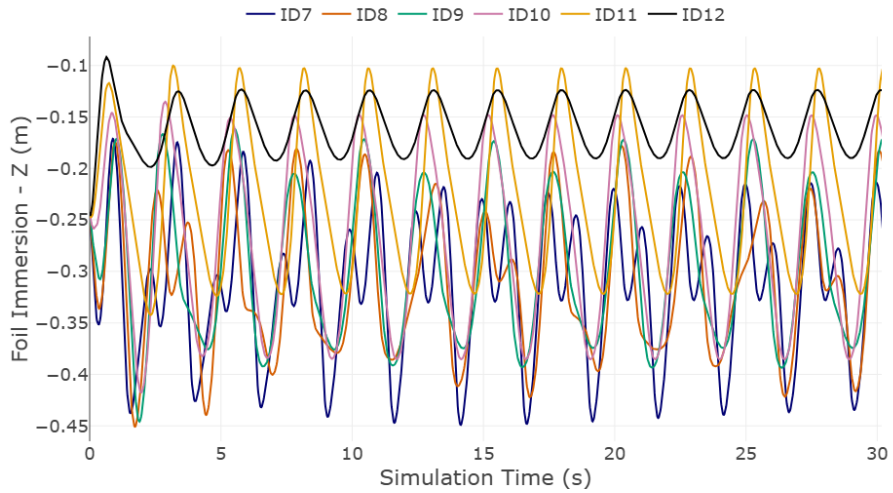


(b)

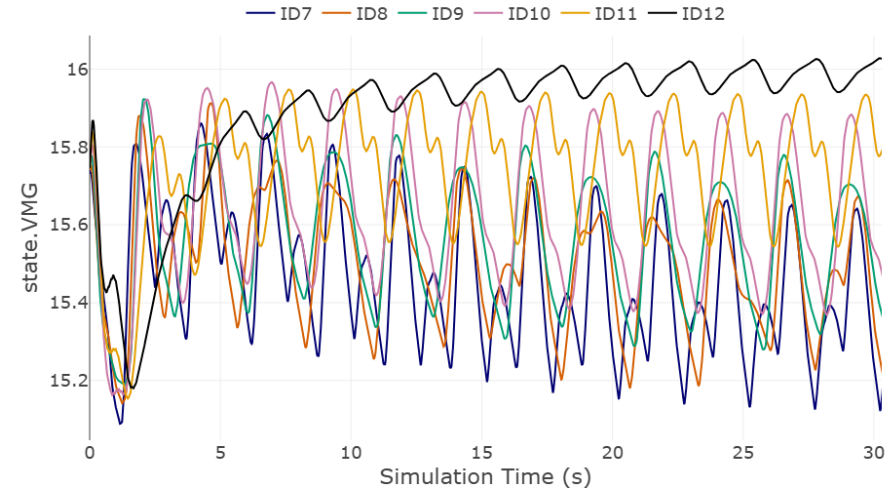


Figure 5.5: Sensitivity of the flight control system to changing gearing ratios in upwind sailing excited by Wave01 (Table 5.2) in terms of foil immersion (Fig. 5.5a) and upwind performance (VMG in kn; Fig. 5.5b). The six gearing ratios tested are shown, increasing progressively from greater ratios (ID1) to smaller response ratios (ID6) (see Table 5.3). The first 30 seconds of each simulation are shown.

***Downwind performance in flat water conditions***

Figure 5.6 shows downwind, flat-water runs. Unlike the upwind case, all gearings converge quickly to a steady flight with no sustained oscillation (Fig. 5.6a). The main effect of gearing here is a bias in the equilibrium ride height, which translates into minor differences in the VMG plateau (Fig. 5.6b). One extreme setting (ID18, Gearing 6) departs from the group and yields a better VMG because it is flying higher with less resistance. Please note that, for simplicity, the VMG represented in the analyses is the upwind VMG. Thus, for downwind testing, it should be taken into account that more negative values correspond to greater downwind VMG.

(a)

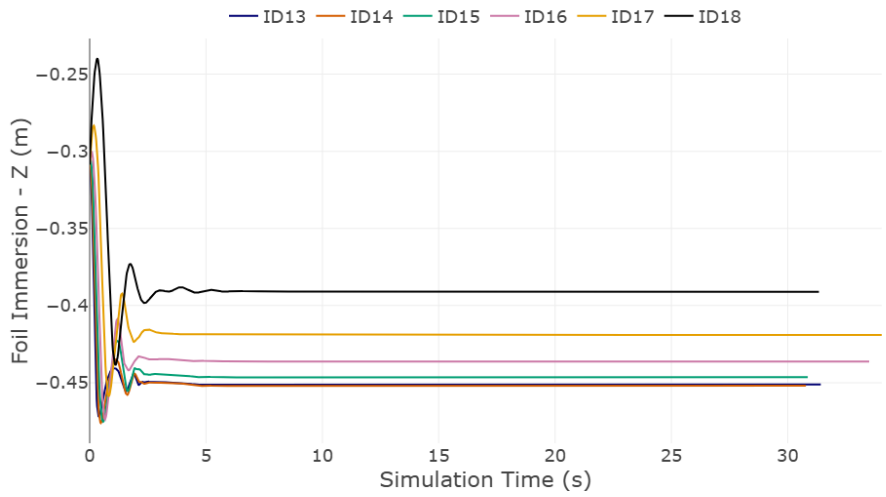


(b)

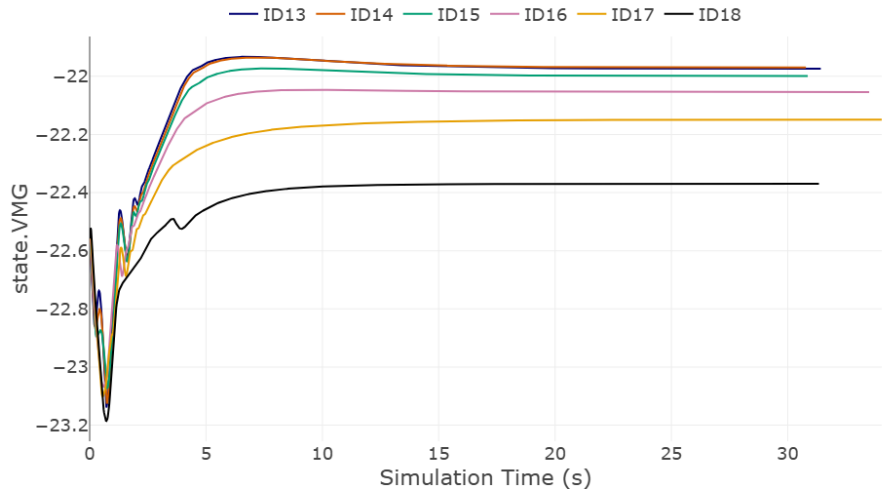


Figure 5.6: Sensitivity of the flight control system to changing gearing ratios in downwind sailing in flat waters conditions in terms of foil immersion (Fig. 5.6a) and downwind performance (VMG in kn; Fig. 5.6b). The six gearing ratios tested are shown, increasing progressively from greater ratios (ID1) to smaller response ratios (ID6) (see Table 5.3). Please note that VMG is not normalised and represents pure upwind VMG, thus more negative values correspond to greater downwind VMG. First 30 seconds of each simulation are shown.

***Downwind performance under regular wave conditions***

Figure 5.5 extends the analysis to runs with Wave01. The response is driven primarily by the wave–encounter frequency: foil immersion oscillates about the ride height (Fig. 5.5a) and VMG exhibits the same modulation (Fig. 5.5b). Differences across gearings appear mainly as changes in oscillation amplitude and a modest shift of the mean level. Lower-response gearings reduce the amplitude of the ride-height and VMG oscillations, whereas the most responsive setting amplifies them and slightly degrades the mean VMG. In this condition, moderate-to-low response gearings are preferred, as they deliver smoother flight with equal or better average performance.

(a)

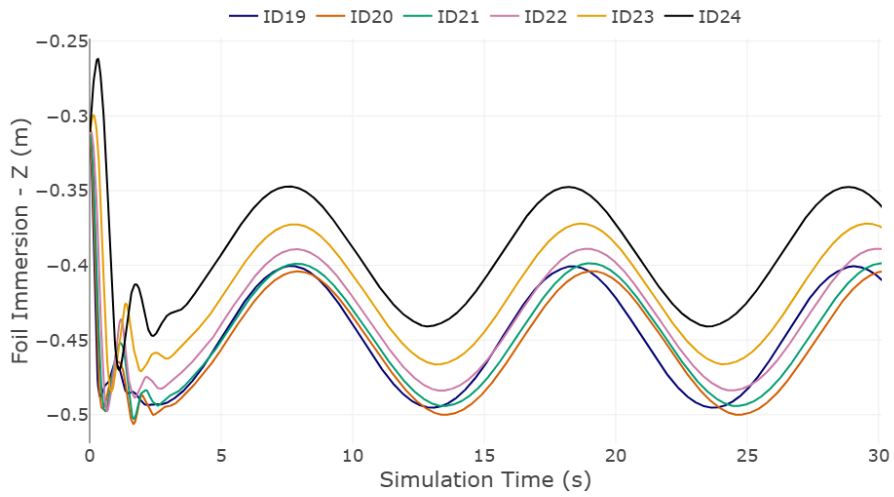


(b)

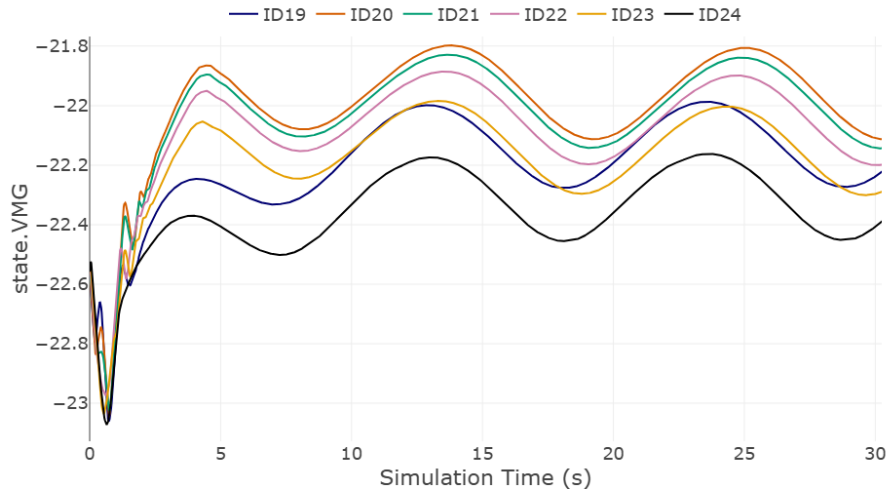


Figure 5.7: Sensitivity of the flight control system to changing gearing ratios in downwind sailing excited by Wave01 (Table 5.2) in terms of foil immersion (Fig. 5.7a) and downwind performance (VMG in kn; Fig. 5.7b). The six gearing ratios tested are shown, increasing progressively from greater ratios (ID1) to smaller response ratios (ID6) (see Table 5.3). Please note that VMG is not normalised and represents pure upwind VMG; thus, more negative values correspond to greater downwind VMG. The first 30 seconds of each simulation are shown.

### 5.3.3 Conclusions of the Mechanical Wand Gearing Study

From the results obtained with the *mechanical* wand–flap system (§ 5.3.2), the following conclusions were drawn:

**G1 Upwind, flat water:** higher–response gearings (larger flap change per degree of wand angle) lead to a lightly damped, near-periodic motion in foil immersion and VMG. The lowest-response gearing (ID6) is the only setting that reaches and maintains a stable ride height.

**G2 Upwind, waves:** the response is dominated by the encounter-frequency forcing. Reducing the gearing lowers the effective loop gain and attenuates the oscillation amplitude in both $z$ and VMG, without penalising the mean level; the lowest-response setting provides the smoothest behaviour.

**G3 Downwind, flat water:** all gearings converge to steady flight with no sustained oscillations. The main effect of gearing is a bias in the equilibrium ride height, reflected in slight shifts of the VMG plateau. All gearings offer stable flight but at different ride heights.

**G4 Downwind, waves:** lower-response gearings reduce the amplitude of the response in $z$ and VMG, whereas the most responsive settings amplify it and can slightly degrade the mean VMG.

**G5 Role of gearing:** within this mechanical scheme, gearing functions as an effective loop-gain *control parameter*. Reducing the response scales down the effective gain and increases damping and robustness to platform couplings (e.g. roll and TWA PIDs), favouring stable flight.

Further work should include the interaction with other control loops, exploring irregular sea states and longer runs, including a more realistic wand model (e.g. the one used by Castañeda, 2018 in [1]), co-tune wand length and *RH offset* to achieve results at the same overall ride height, and compare against on-water data to calibrate the gearing map.

## 5.4 Wand Length Sensitivity

In the mechanical wand–flap system, the wand length is a primary geometric parameter. It sets the lever arm with which the free surface is "sampled" and, together with the *RH offset* (bias), determines the mean wand incidence required to achieve a given ride height. In practice, sailors use wand length mainly to influence the average ride height and the system's sensitivity to surface undulations; when combined with *RH offset*, it effectively controls the equilibrium wand angle. In this study, we isolate the effect of varying wand length, holding all other settings constant.

We quantify how changes in wand length affect (i) the mainfoil immersion $z$ (as a proxy for ride height), (ii) the wand angle time history, and (iii) the resulting VMG, across upwind and downwind conditions, in flat water and under a simple regular wave (Wave01; Table 5.2).

### 5.4.1 Analysis

We run a matrix of simulations in which the wand length is varied from 0.70 m to 1.20 m in 0.10 m steps, keeping the gearing fixed (Setting 3) and the initial conditions from the VPP at TWS = 14 kn (§ 5.2). Each case is executed in upwind and downwind, both in flat water and under Wave01 (Table 5.2). The complete list of runs (IDs 25–48) is provided in Table 5.4. All simulations are at least 60 s long to ensure convergence to steady (or periodic) behaviour; for clarity, figures report the first 30 s.

Table 5.4: Details of the simulations performed in § 5.4

| Simulation ID# | Condition | Waves | Gearing | Wand Length (m) |
|---|---|---|---|---|
| 25 | Upwind | Flat | 3 | 0.7 |
| 26 | Upwind | Flat | 3 | 0.8 |
| 27 | Upwind | Flat | 3 | 0.9 |
| 28 | Upwind | Flat | 3 | 1.0 |
| 29 | Upwind | Flat | 3 | 1.1 |
| 30 | Upwind | Flat | 3 | 1.2 |
| 31 | Upwind | Wave01 | 3 | 0.7 |
| 32 | Upwind | Wave01 | 3 | 0.8 |
| 33 | Upwind | Wave01 | 3 | 0.9 |
| 34 | Upwind | Wave01 | 3 | 1.0 |
| 35 | Upwind | Wave01 | 3 | 1.1 |
| 36 | Upwind | Wave01 | 3 | 1.2 |
| 37 | Downwind | Flat | 3 | 0.7 |
| 38 | Downwind | Flat | 3 | 0.8 |
| 39 | Downwind | Flat | 3 | 0.9 |
| 40 | Downwind | Flat | 3 | 1.0 |
| 41 | Downwind | Flat | 3 | 1.1 |
| 42 | Downwind | Flat | 3 | 1.2 |
| 43 | Downwind | Wave01 | 3 | 0.7 |
| 44 | Downwind | Wave01 | 3 | 0.8 |
| 45 | Downwind | Wave01 | 3 | 0.9 |
| 46 | Downwind | Wave01 | 3 | 1.0 |
| 47 | Downwind | Wave01 | 3 | 1.1 |
| 48 | Downwind | Wave01 | 3 | 1.2 |

### 5.4.2 Results

Elongating the wand length from 70 cm to 120 cm had substantial effects on the sailing performance of the International Moth simulator, as expected according to real sailing conditions. **Note for downwind testing**: The VMG presented in this section is not normalised, so even though it has a negative sign, only the absolute value (magnitude) must be taken into account.

***Upwind performance in flat water conditions***

Figure 5.8 documents the effect of *wand length* in upwind, flat water.

Increasing `parameter.wand_length` produces a clear, nearly monotonic shift of the mean ride height: longer wands fly higher (smaller immersion magnitude) for the same *RH offset*, as seen in the steady levels of $z$ (Fig. 5.8a). The steady wand angle achieves a standard value close to the one imposed by the bias adjuster; this supports the hypothesis that lengthening the wand mainly adjusts the mean ride height until the system re-establishes approximately the same equilibrium wand angle (Fig. 5.8b). One extreme case does not settle and instead exhibits a bounded limit cycle in both $z$ and wand angle, similar to the oscillatory behaviour observed with the most responsive gearings in upwind–flat runs.

In terms of performance, VMG broadly follows ride height (Fig. 5.8c): the shortest wand, which flies very close to the water, attains the lowest plateau, consistent with increased drag; whereas intermediate/longer lengths achieve higher plateaus.

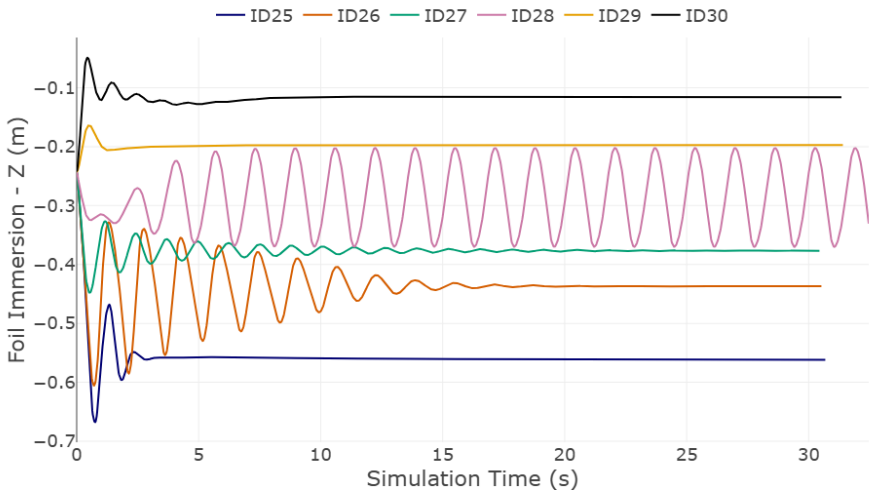


(a)

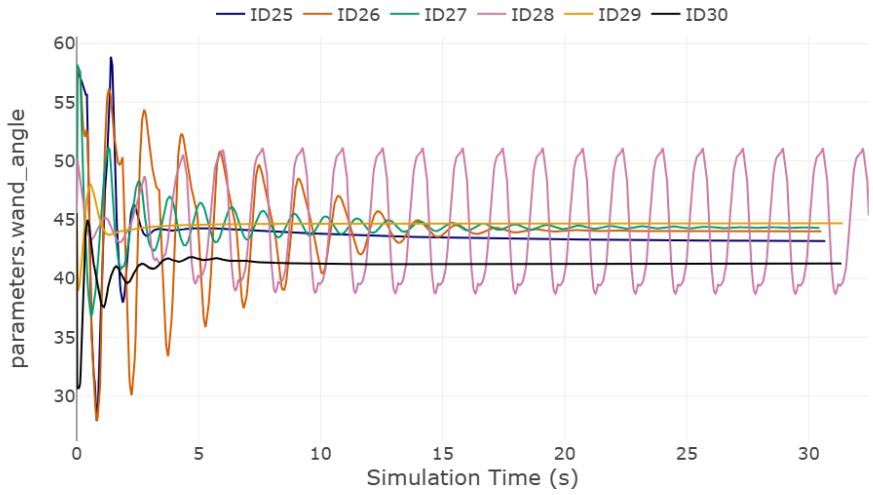


(b)

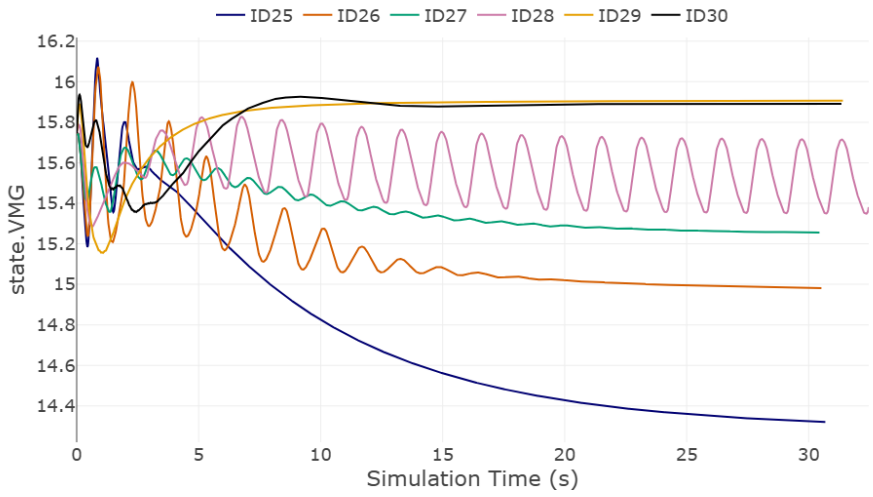


(c)

Figure 5.8: Sailing responses to modifying wand length in terms of foiling immersion (a), wand angle (b) and upwind VMG (c, in knots) in flat water conditions. Six wand lengths were tested, from 70 cm to 120 cm (ID25 to ID30, respectively)

***Upwind performance under regular wave conditions***

Figure 5.9 shows the effect of wand length under Wave01. The response is locked to the encounter frequency in all cases: foil immersion oscillates periodically (Fig. 5.9a) and the wand angle exhibits the corresponding modulation (Fig. 5.9b). Increasing wand length shifts the mean ride height upwards (smaller immersion magnitude) and tends to increase the oscillation amplitude, whereas shorter wands fly lower and decrease slightly those amplitudes. After a brief transient of about 5 seconds, all runs settle into bounded periodic motion with no loss of stability.

(a)

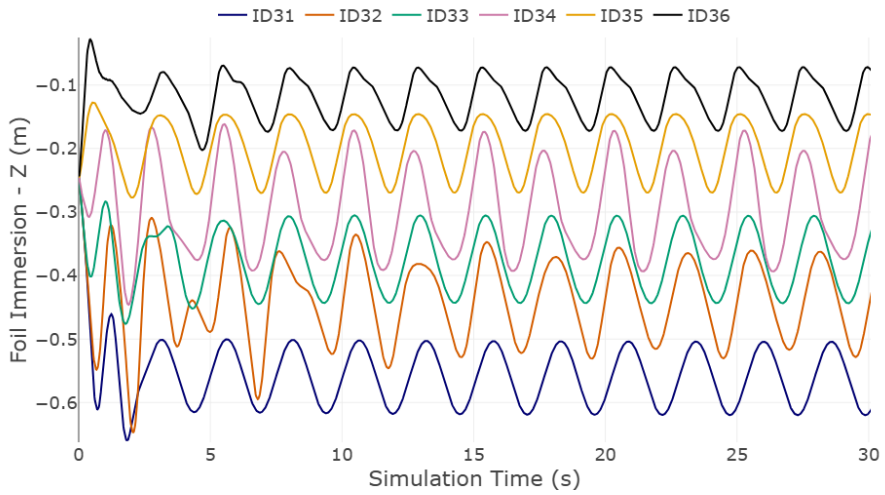


(b)

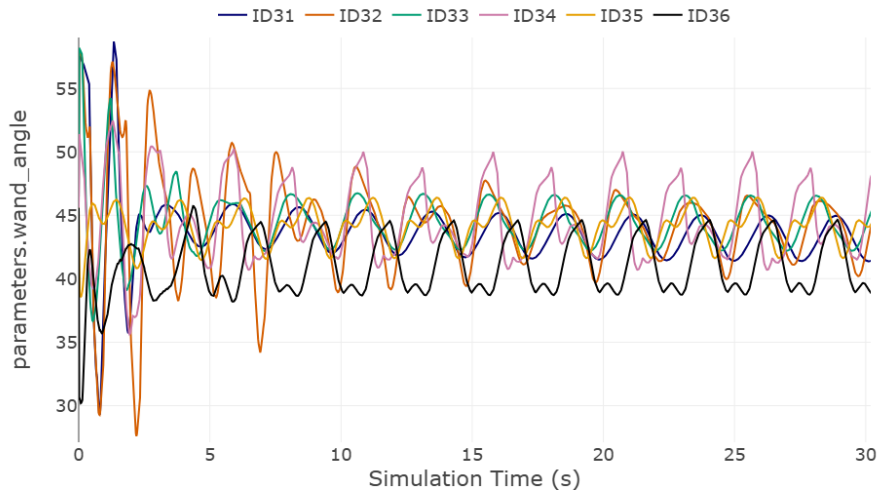


Figure 5.9: Upwind sailing responses to modifying wand length in terms of foiling immersion (a) and wand angle (b) under Wave01. Six wand lengths were tested, from 70 cm to 120 cm (ID25 to ID30, respectively)

***Downwind performance in flat water conditions***

Figure 5.10 shows that, in downwind flat conditions, varying the wand length mainly biases the equilibrium ride height while dynamics remain well damped: both $z$ (Fig. 5.10a) and the wand angle (Fig. 5.10b) converge rapidly. The *signed* downwind VMG plateaus (Fig. 5.10c) become *more negative* as wand length increases (drag reduces) whereas the shortest wand, which flies closest to the water, attains the smaller velocity vector projected downwind.

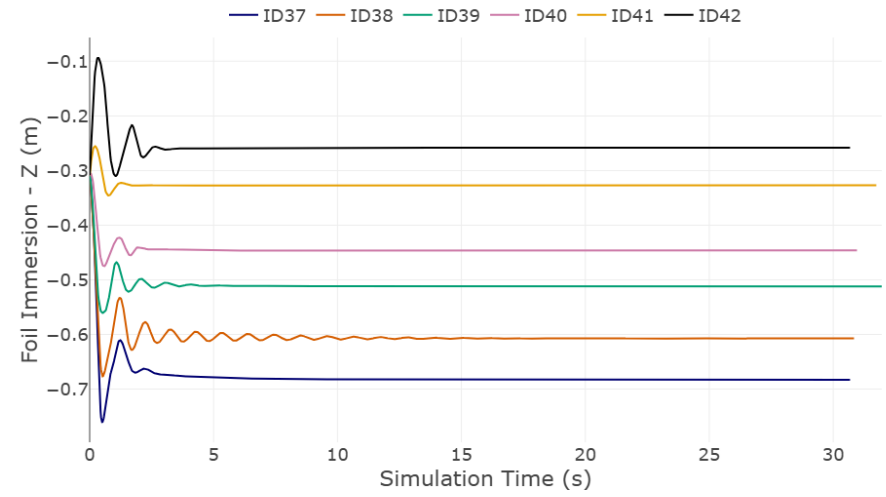


(a)

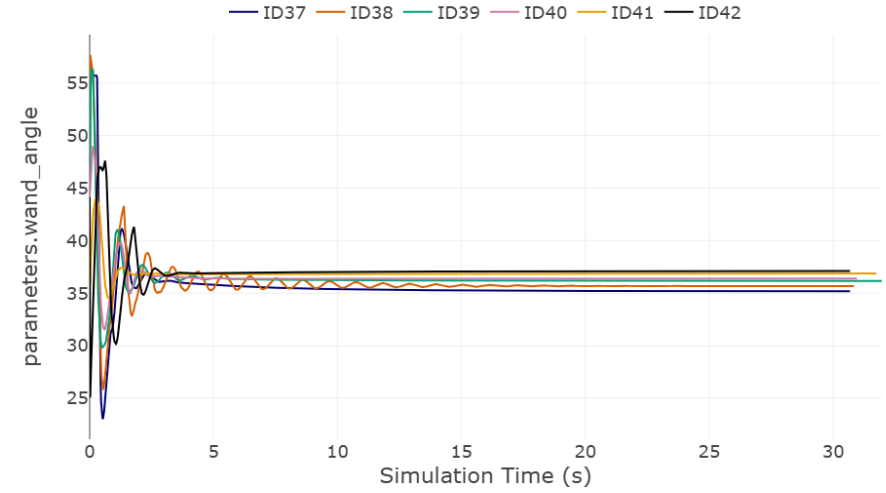


(b)

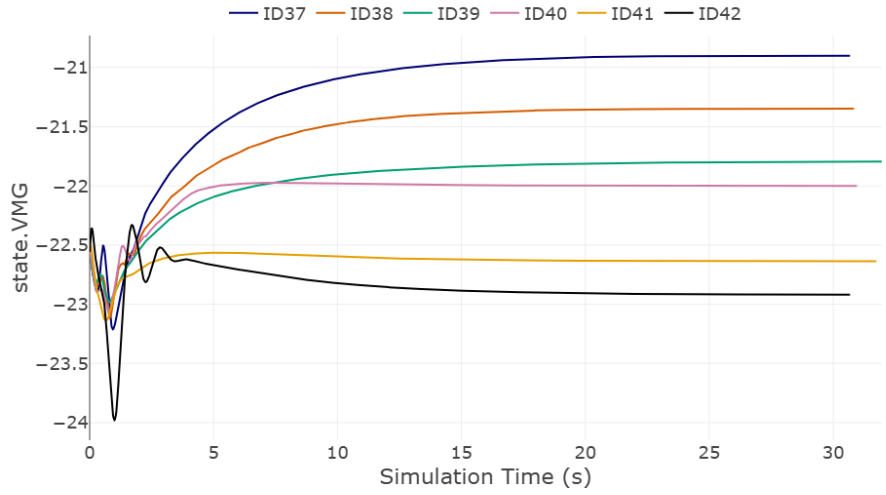


(c)

Figure 5.10: Sailing responses to modifying wand length in terms of foiling immersion (a), wand angle (b) and downwind VMG (c, in knots, take absolute value) in flat water. Six wand lengths were tested, from 70 cm to 120 cm (ID37 to ID42, respectively)

***Downwind performance under regular wave conditions***

Figure 5.11 repeats the analysis with Wave01. The ride height tracks the wave at the encounter frequency in all cases (Fig. 5.11a), while the wand angle remains narrowly modulated around its steady value (Fig. 5.11b). As in flat water, increasing $L_{\text{wand}}$ primarily raises the mean flight level; the influence on oscillation amplitude is modest and secondary to the wave forcing. Overall, wand length acts as a height control of the mean downwind flight in waves, with all tested settings exhibiting stable, bounded periodic behaviour.

(a)

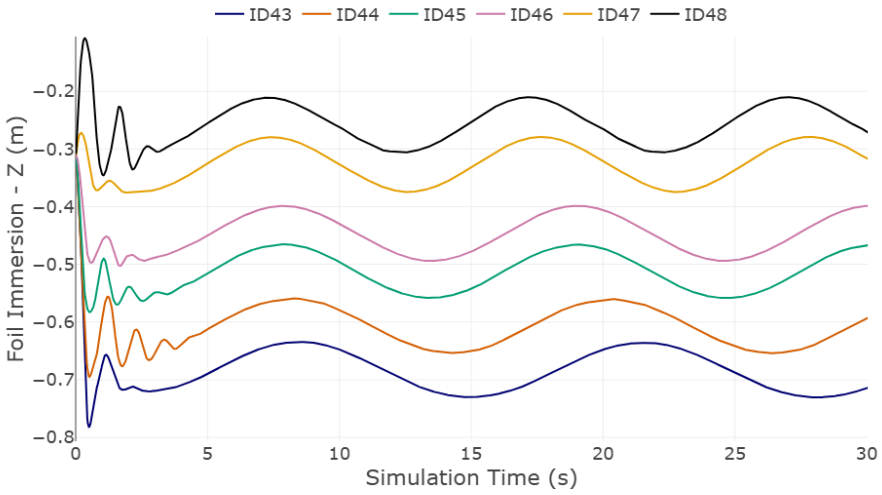


(b)

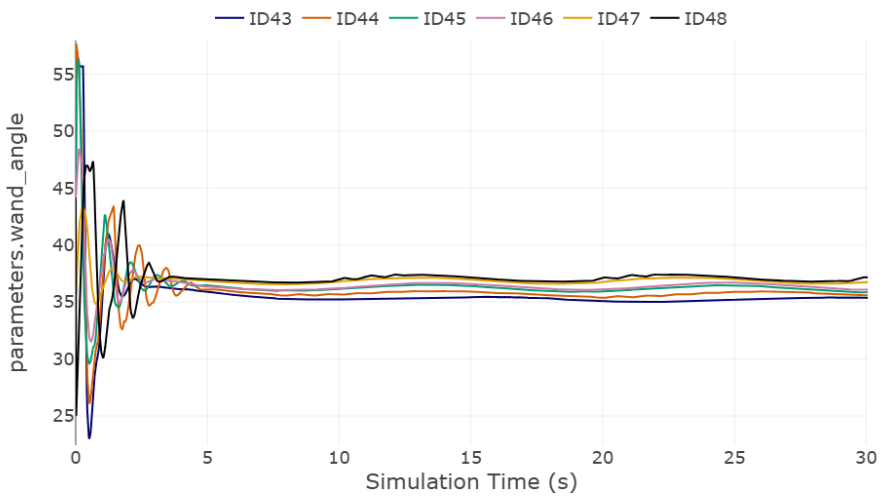


Figure 5.11: Downwind sailing responses to modifying wand length in terms of foiling immersion (a) and wand angle (b) under Wave01. Six wand lengths were tested, from 70 cm to 120 cm (ID43 to ID48, respectively)

### 5.4.3 Conclusions of the Wand Length Study

From the results obtained in § 5.4, the following conclusions were drawn:

**WL1 Geometric role.** Varying wand length primarily biases the *mean* ride height while the steady wand angle stabilizes around a common value. This is consistent with the trigonometry that defines the push rod system.

**WL2 Upwind—Flat Water.** Increasing wand length raises the mean flight level (smaller immersion magnitude). All lengths except the $L_{\text{wand}} = 1.0\ m$ settle to steady flight; the longest case exhibits a bounded limit cycle in $z$ and in the wand angle.

**WL3 Upwind—Regular Wave.** Longer wands shift the mean flight level upward and tend to increase the oscillation amplitude; all cases remain stable with bounded periodic motion.

**WL4 Downwind—Flat Water.** Dynamics are well damped for all lengths. The signed downwind VMG becomes progressively *more negative* as $L_{\text{wand}}$ increases, indicating better performance with higher flight - consistent with hydrodynamic models.

**WL5 Downwind—Regular Wave.** Changes in oscillation amplitude are small relative to the wave forcing and all runs remain stable.

Further work should include joint tuning of wand length with *RH offset* and gearing in order to evaluate the effects of wand angle, incorporation of realistic wand dynamics (shockcords, springs, dampers and friction), tests in irregular seas and longer runs, and comparison with on-water measurements.

## 5.5 Heave PID Controller Study

In this section, I tested the sensitivity of the simulator controlled by the PID to changes in the values of Kp, Ki and Kd. For that purpose, the first step was tuning the heave proportional–integral–derivative controller (PID) built in § 3.2.5, changing the values of Kp, Ki, and Kd independently until achieving a stable flight. Once a stable upwind flight was achieved with the PID (after performing more than 300 runs), the values of those K variables were stored as *base* Kp, Ki and Kd. Finally, we conducted new simulator runs with slight changes to the PID's base parameters and to the environmental conditions and analysed the response variables, providing information on sailing performance. The output variable that was studied as a proxy of boat performance was the vertical foil immersion (m)—some other output variables from the simulator, such as the `auto.flap` parameter, wand angle, or VMG were plotted and checked, but not subjected to analysis.

### 5.5.1 Analysis

For simplifying this study, we assumed that the base value was the correctly tuned value. To observe the effects of each potential gain, an undertuned, a tuned and an overtuned value were tested while maintaining the rest of the PID variables in the base value. These tests were performed for flat water (for 30 s) and excited by Wave01 (for 60 s), always in Upwind Conditions. The values of K parameters and the conditions tested are presented in the following Table 5.5:

Table 5.5: Values of Kp, Ki and Kd that will be used for simulations in the Heave PID Controller Study (§ 5.5)

| | Undertuned | Tuned | Overtuned |
|---|---|---|---|
| Kp | 1.0 | 4.0 | 8.0 |
| Ki | 1.0 | 2.0 | 3.0 |
| Kd | 3.0 | 6.0 | 9.0 |

The simulations run are presented in Table 5.6.

Table 5.6: Details of the 18 simulations performed in the Heave PID Controller Study (§ 5.5)

| Simulation ID# | Condition | Waves | Kp | Ki | Kd |
|---|---|---|---|---|---|
| 49 | Upwind | Flat | 1 | 2 | 6 |
| 50 | Upwind | Flat | 4 | 2 | 6 |
| 51 | Upwind | Flat | 8 | 2 | 6 |
| 52 | Upwind | Wave01 | 1 | 2 | 6 |
| 53 | Upwind | Wave01 | 4 | 2 | 6 |
| 54 | Upwind | Wave01 | 8 | 2 | 6 |
| 55 | Upwind | Flat | 4 | 1 | 6 |
| 50 | Upwind | Flat | 4 | 2 | 6 |
| 57 | Upwind | Flat | 4 | 3 | 6 |
| 58 | Upwind | Wave01 | 4 | 1 | 6 |
| 53 | Upwind | Wave01 | 4 | 2 | 6 |
| 60 | Upwind | Wave01 | 4 | 3 | 6 |
| 61 | Upwind | Flat | 4 | 2 | 3 |
| 50 | Upwind | Flat | 4 | 2 | 6 |
| 63 | Upwind | Flat | 4 | 2 | 9 |
| 64 | Upwind | Wave01 | 4 | 2 | 3 |
| 53 | Upwind | Wave01 | 4 | 2 | 6 |
| 66 | Upwind | Wave01 | 4 | 2 | 9 |

### 5.5.2 Results

Figure 5.12 shows the foil immersion for upwind conditions in flat water versus wavy conditions. The foil immersion curves illustrate the typical shape that the heave response adopts: (i) A first bump until the simulation equilibrium and the PID converges, and then a horizontal line maintaining a stable flight in flat water - with a properly trimmed PID. (ii) In waves, the boat is excited up and down following the wave, and stabilises around the equilibrium ride height oscillating periodically (in the case of ID-53, with a noticeable lower amplitude and period (0.005 m, 2.5 s) than the wave (0.5 m, 5 s), the latter due to the effects of the boat speed in the wave encounter frequency).

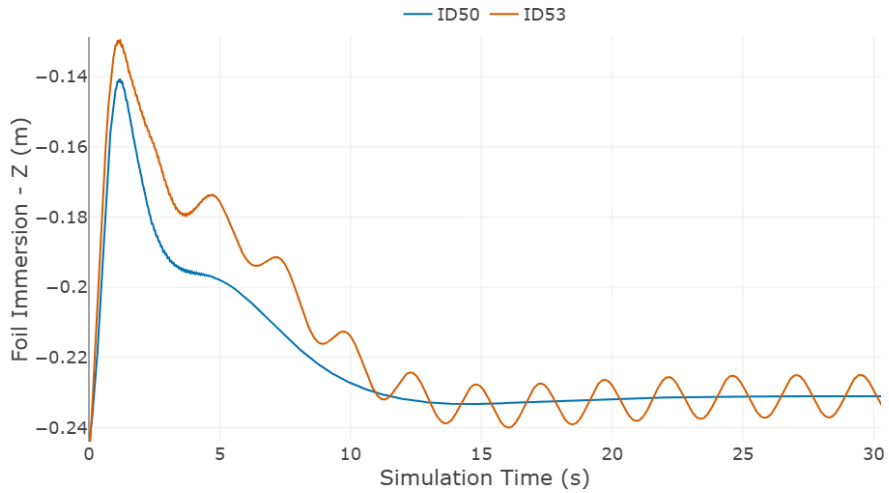


Figure 5.12: Typical trend of height of flight (measured through the foil immersion) with the PID-controlled simulator for upwind conditions in flat water (blue line, ID-50) and with the model Wave 01 (orange line, ID-53).
The figure shows the first 30 seconds of simulation.

***Modifying the base Kp value***

Figure 5.13 presents the sensitivity of the flight-control system to the proportional gain ($K_p$), measured by the foil immersion $z$. With a low gain ($K_p = 1$) the return to the equilibrium ride height is slow and the transient deviation is larger. With a high gain ($K_p = 8$) the initial correction is faster but produces marked overshoot and sustained oscillations; this is more evident in seastate conditions (Fig. 5.13c). The reference gain ($K_p = 4$) offers a balanced response, with acceptable rise time, limited overshoot, and the smallest steady oscillation in both flat water (Fig. 5.13b) and waves (Fig. 5.13c). Overall, the results confirm the expected trade-off between responsiveness and damping when tuning the proportional action of the PID controller.

(a)

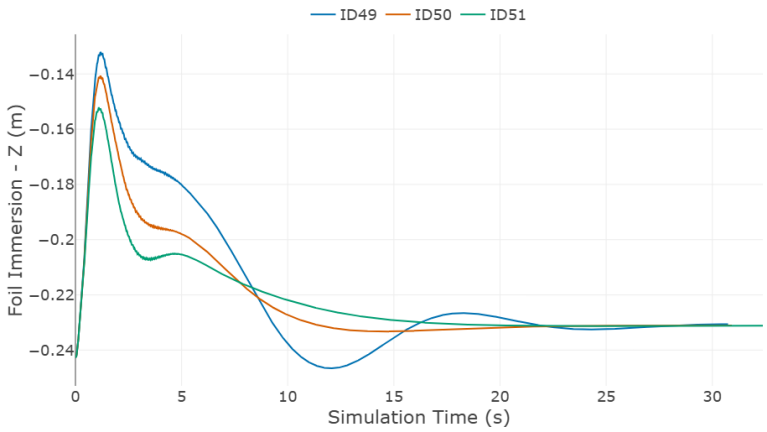


(b)

(c)

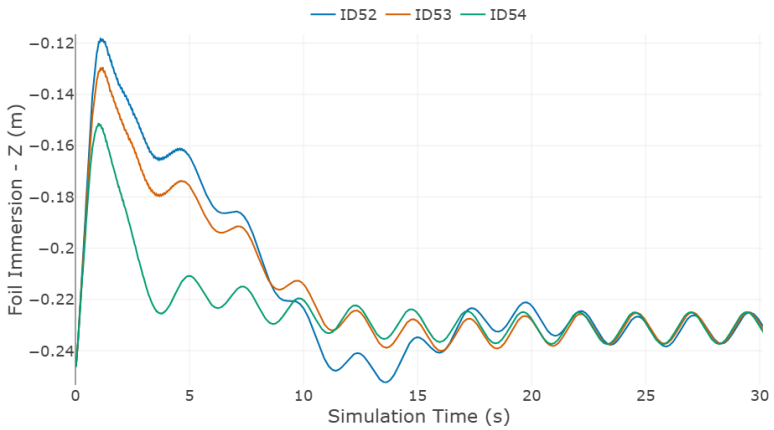


Figure 5.13: Response of the designed flight control system to changing values, measured as foil immersion. The foil immersion acts as a reference parameter to describe the heave motion and the performance achieved by the heave PID controller. The orange line (Simulation ID50, as in Table 5.6) corresponds to a PID with the base Kp value (Kp = 4); The blue line (Simulation ID49) corresponds to a undertuned value of Kp (Kp = 1); and the green line (Simulation ID51) with a overtuned Kp (Kp = 8).

***Modifying the base Ki value***

Figure 5.14 examines the effect of the integral gain ($K_i$) on the foil immersion $z$. A low gain ($K_i = 1$) delays the removal of the bias and leads to the longest settling time in both flat water (Fig. 5.14a) and waves (Fig. 5.14b). Increasing the gain to $K_i = 3$ accelerates the return to the target ride height and does not amplify the oscillations with respect to the reference case ($K_i = 2$); its convergence is faster in both conditions. Within this envelope, $K_i = 3$ is therefore a suitable candidate to improve the PID tuning, delivering faster convergence with no adverse side effects observed.

(a)

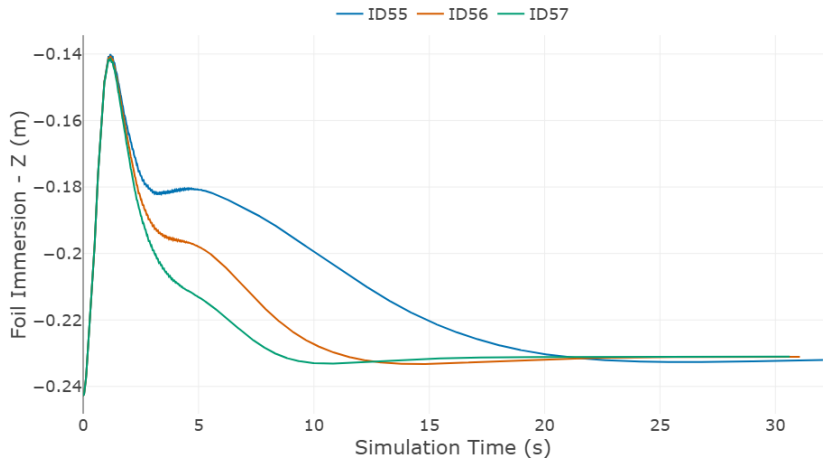


(b)

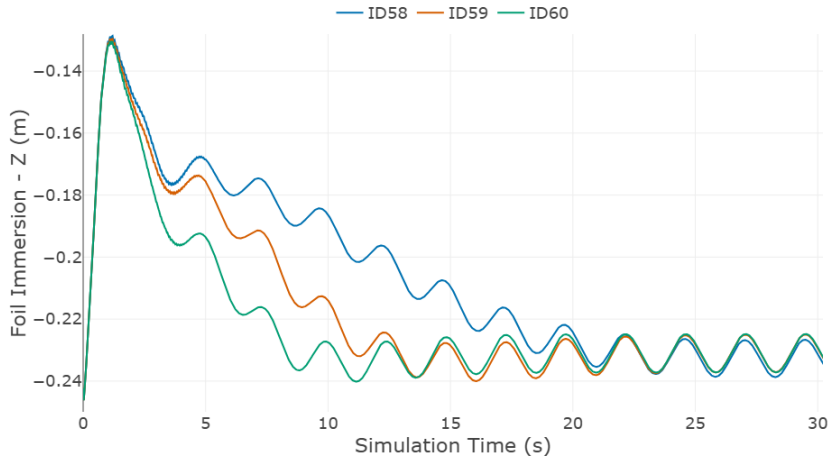


Figure 5.14: Response of the designed flight control system to changing values, measured as foil immersion.
The orange line (Simulation ID56) corresponds to a PID with the base Ki value (Ki = 2); The blue line (Simulation ID55) corresponds to a undertuned value of Ki (Ki = 1); and the green line (Simulation ID57) with a overtuned value (Ki = 3).
A low value of Ki (blue line) substantially increases the time it takes for the boat to reach the foil immersion target both in flat water (a) and with Wave01 (b).

***Modifying the base Kd value***

Figure 5.15 evaluates the effect of the derivative gain ($K_d$) on the foil immersion $z$. In flat water (Fig. 5.15a), a low gain ($K_d = 3$) yields a slightly slower and less damped approach to the target than the base value ($K_d = 6$). In seastate (Fig. 5.15b), the benefit of increasing $K_d$ from 3 to 6 is clearer: the periodic oscillation around the ride-height target is reduced. Pushing the derivative action further ($K_d = 9$) becomes counterproductive under waves, with amplified oscillations and a loss of damping relative to the base case. Within this envelope, $K_d = 6$ provides the best compromise, offering adequate damping without the amplification observed for the overtuned configuration.

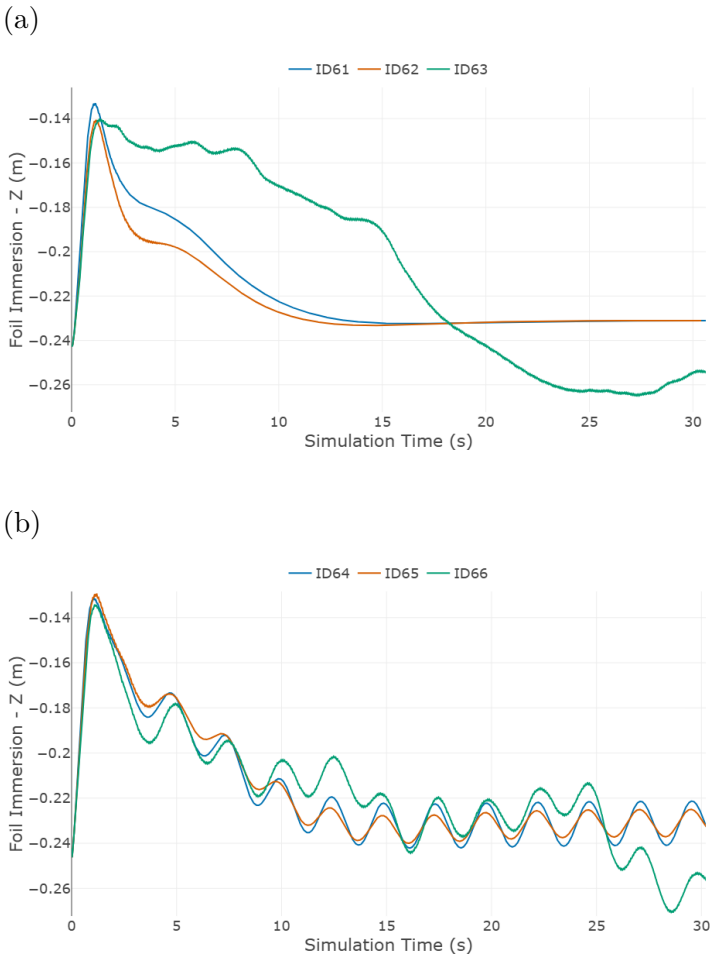


Figure 5.15: Response of the flight control system to changing values.
The orange line (Simulation ID62) corresponds to a PID with the base Kd value (Kd = 6); The blue line (ID61) corresponds to a undertuned value (Kd = 3); and the green line (ID63) with a overtuned value (Kd = 9).
A low value of Kd (blue line) slightly increases the time it takes for the boat to reach the foil immersion target both in flat water (a). In (b), with seastate, the effects of increasing Kd from the undertuned to the base are more visible: the amplitude of the periodic oscillation around the target is reduced. Also (b), illustrates the risks of a overtuned Kd, the oscillations are amplified.

### 5.5.3 Conclusions of the Heave PID Controller Study

From the presented results of the PID controlled flight (in § 5.5.2), the following conclusions were drawn:

**PID1** Within the tested range, the baseline gains provide the best compromise between responsiveness and damping: increasing Kp above the base value shortens the rise time but introduces larger overshoot and persistent oscillations (more evident under seastate), whereas reducing $K_p$ slows convergence and enlarges the transient deviation. Likewise, Kd below the base value results in a slower, less damped approach to the target, while $K_d$ above the base amplifies wave-induced oscillations and erodes damping. Hence, the baseline $K_p$ and $K_d$ are near-optimal for upwind conditions tested.

**PID2** Raising the integral gain (Ki) improved bias removal and settling without triggering oscillations in the explored envelope: $K_i = 3$ outperformed the baseline $K_i = 2$ in both flat water and waves. This indicates that the baseline integral action is conservative and can be increased; a broader sweep (with integral anti-windup/clamping) is recommended to identify the upper safe bound.

**PID3** Overall, the PID controller achieved stable upwind flight. The simulator captured the key physics well enough that the outputs matched the expected trends of the PID variables [36]. Through developing and testing this system, I gained substantial practical experience.

Further studies could include testing in downwind conditions, other attitudes, multiple sea-states and combined variable perturbations at the same time.

## 5.6 Comparison between the Wand Mechanism and the heave PID

In this section, an initial comparison is established between the two flight control systems.

### 5.6.1 Analysis

The outputs of the upwind simulations, both in flat water and with seastate, are presented together for both flight control systems, using simulation runs already performed in former sections § 5.3 & § 5.5.

### 5.6.2 Results

Figure 5.16 compares the tuned PID controller with the mechanical wand–flap system in upwind sailing. In panel (a) (flat water), the tuned PID (ID50) converges rapidly to the target immersion with minimal overshoot and no residual oscillations. The wand mechanism with a low-response gearing (ID6) also attains a steady flight, but with a small steady bias relative to the target. In contrast, the higher-response gearing (ID4) exhibits a periodic cycle: foil immersion oscillates with nearly constant amplitude after the initial transient.

Under Wave01 (panel (b)), all cases oscillate at the encounter frequency, but with markedly different attenuation. The PID achieves the smallest motion envelope around the mean immersion, the low-response wand (ID12) shows intermediate amplitude, and the higher-response wand (ID10) tracks the wave most strongly and presents the largest excursions.

(a) Foil immersion is plotted for the first 30 seconds of simulation for three runs: ID4 (Upwind-Flat Water-Wand Mechanism-Gearing 4), ID6 (Upwind-Flat Water-Wand Mechanism-Gearing 6) and ID50 (Upwind - Flat Water-Tuned PID)

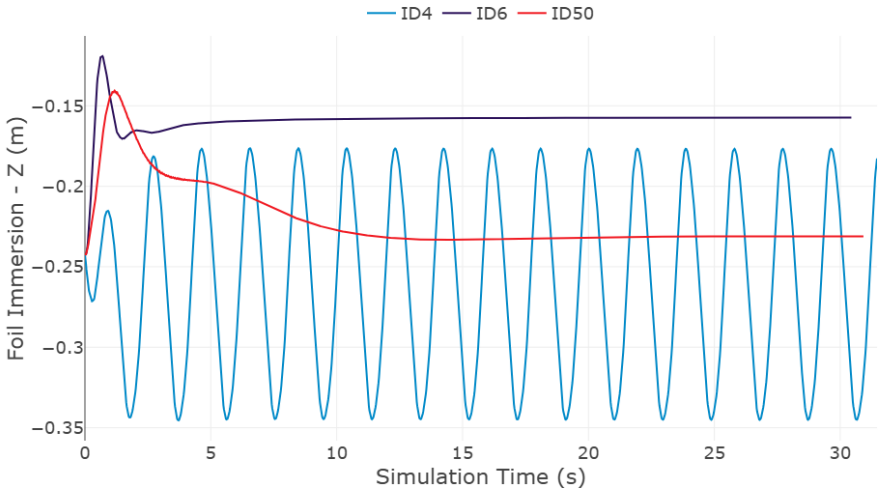


(b) Foil immersion is plotted for the first 30 seconds of simulation for three runs: ID4 (Upwind-Wave01-Wand Mechanism-Gearing 4), ID6 (Upwind-Wave01-Wand Mechanism-Gearing 6) and ID50 (Upwind-Wave01-Tuned PID)

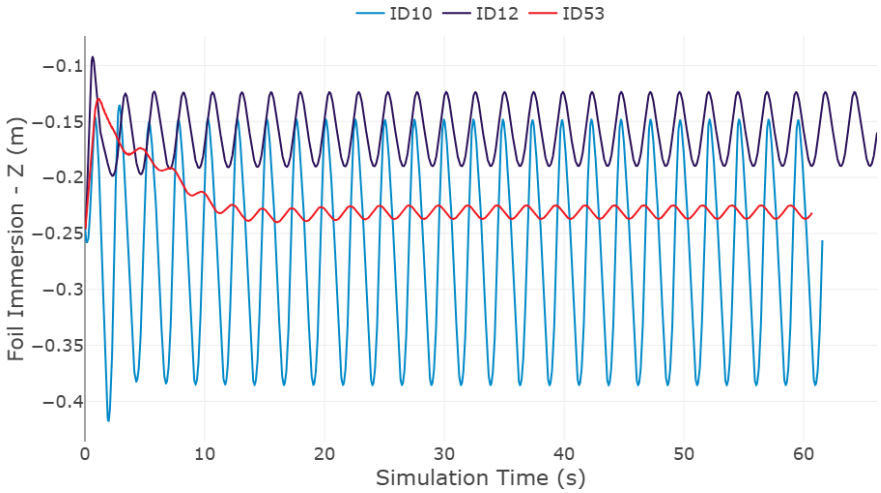


Figure 5.16: Comparison between PID and Wand system behaviour in upwind conditions

### 5.6.3 Conclusions and discussion of the comparison

Across flat-water and wave conditions, the tuned PID exhibits the shortest settling time and the best disturbance rejection. The mechanical wand–flap system, in contrast, trades attenuation for simplicity and deliberate "wave following," with its behaviour principally set by the gearing (lower response ⇒ lower effective loop gain and higher damping). In practical terms, this margin translates into a real on-water advantage for the PID pathway: tighter ride-height control reduces unnecessary drag and keeps aero/hydro trim steadier—especially in waves—yielding more repeatable performance and easier boat handling.

From an engineering standpoint, these early results are encouraging for a control-based solution. By replacing the water-contact wand and using an electronic ride-height sensor, the PID pathway removes wand-induced free-surface disturbance and local drag upstream of the mainfoil. The evidence supports continued development and on-water validation of the PID approach (robust tuning, anti-windup, sensor/IMU fusion, actuator-limit handling); the mechanical wand remains a simple, low-risk option with proven reliability.

That said, several limitations apply. First, the present tests cover a limited envelope; the PID performance should be studied across the full operating range, including challenging scenarios (large sea state, manoeuvres and bear-aways). Furthermore, an ergonomic, fail-safe method for on-water tuning should be designed to avoid accidental mistuning. Second, the mechanical wand has a 20-year track record across all conditions; the PID approach, although promising, requires sustained testing before it can match that operational maturity. Finally, electronic ride-height sensing and control are currently prohibited by the International Moth Class Rules [3]; any benefits will remain theoretical for official racing until the technology is widely validated (outside regattas) and permitted by the class.

# 6.

# Conclusions

**Summary.** This MSc project assembled an operational International Moth test platform inside *Simulator in Motion* (SiM), aligned inputs with a reference D3-VPP solution, and exercised two flight-control approaches—mechanical wand and a heave PID—through sensitivity studies in flat water and a simple regular seastate. The simulator reproduced the VPP targets at two representative operating points (upwind/downwind, TWS = 14 kn) within tight acceptance bands for primary performance and attitudes, validating the platform as a credible environment for controller studies within the tested envelope.

## Main findings

1. **Simulator - VPP consistency at 14 kn.** In upwind, speed and VMG matched D3-VPP within +0.46% and +1.36%, with heel on target, pitch offset small, and ride height on the VPP mark; main-foil forces agreed to within $\sim 5\%$ and overall residuals were near zero (Table 4.1). In downwind, $V_s$ and VMG were within +0.34% and 0.72%, attitudes close to target with a small nose-down pitch, ride height within 0.011 m, and equilibria clean (Table 4.3). The largest differences across both points appear in control settings and y-axis forces and moments.

2. **Mechanical wand — *gearing* sensitivity.** In upwind waves, reducing gearing (lower response) lowered the effective loop gain and attenuated oscillation amplitude in ride height and VMG without penalising the mean; in downwind, all gearings reached steady flight in flat water, while in waves the higher-response settings amplified periodic motion. Overall, gearing acts as an effective loop-gain control for the mechanical loop.

3. **Mechanical wand — length sensitivity.** Varying wand length primarily biases the mean ride height while the steady wand angle tends to a common value (geometric effect of the push-rod linkage). In all conditions, longer wands raised the mean flight level. In downwind, dynamics were better damped than in upwind for all lengths. Results serve as a perfect example to show how higher flight correlated with improved VMG.

4. **Heave PID study.** A baseline upwind tuning near $K_p = 4$, $K_i = 2$, $K_d = 6$ provided the best compromise in the tested range: increasing $K_p$ shortened rise time

at the expense of overshoot/oscillation (more visible under waves), while reducing $K_p$ slowed convergence. Raising $K_i$ to 3 improved bias removal and settling without adverse oscillations; $K_d$ below the base reduced damping and above the base amplified wave-induced oscillations.

5. **PID vs. wand comparison.** In upwind, the tuned PID showed the shortest settling time and best disturbance rejection in flat water and waves. The wand trades attenuation for simplicity and behaviour dominated by gearing (lower response ⇒ higher damping). This margin translates into steadier aero/hydro trim and easier handling for the PID pathway in the tested scenarios.

# Implications

- **Use of SiM for control design.** Given the close agreement to D3-VPP at 14 kn upwind/downwind and the coherent internal balances, SiM can be used with confidence for flight-control studies, parameter sensitivities and qualitative design iteration around these operating points.

- **Controller practice and tuning.** For the wand, prefer lower-response gearing in waves to attenuate heave/VMG oscillations; for the PID, moderate $K_p$ and $K_d$ with slightly higher $K_i$ (with anti-windup) is a promising direction, always within the tested envelope.

- **Regulatory context.** Electronic ride-height control is presently prohibited in the International Moth Class; hence, any on-water gains from a PID pathway (e.g., removing wand-induced disturbance upstream of the main foil) remain outside official racing until broadly validated and permitted by the class.

# Limitations

This project deliberately constrained its scope: two operating points at TWS = 14 kn (best-VMG upwind/downwind), flat water and a single regular head-sea wave; tuning emphasised achieving a stable flight rather than global optimisation of all PIDs; and the SiM aero model differs from the VPP's Moth-oriented aero, which helps explain discrepancies in control angles and lateral load split. Results therefore apply to the tested craft configuration and the vicinity of these conditions.

# Recommendations and future work

- **Broaden the envelope:** sweep TWS/TWA and sea states (direction, period, irregular spectra) and search for resonances/RAOs; extend studies to downwind PID tuning and attitude combinations (heel/pitch).
- **Controllers:** for the PID, pursue robust tuning with integral anti-windup, and *fail-safe* on-water tuning interfaces; for the wand, enrich the mechanism model (springs, shock-cord, damping, friction) and co-tune length, offset and gearing at matched ride height.
- **Validation:** replicate the SiM–VPP comparison over a matrix of conditions and, where possible, benchmark against on-water measurements to calibrate the gearing map and PID settings.

**Concluding remark.** Within the stated limits, the platform meets its objectives: (i) it reproduces VPP targets credibly, (ii) it captures the expected physics and controller trends (gearing, wand length, PID gains), and (iii) it provides a practical, repeatable bench for advancing Moth flight-control design. This justifies using SiM as a development tool while continuing to expand the envelope and tighten the link to on-water data.

# References


[1] I. Castañeda Sabadell, "Design of a physical and interactive real-time simulator based on a dynamic vpp as a support tool for sailing yacht design and operation," Ph.D. dissertation, ETSI Navales, Universidad Politécnica de Madrid, 2018.

[2] J. Ozanne, *Team principal at simulator in motion, simulator and a.i. team lead at alinghi red bull racing*, https://www.linkedin.com/in/josephozanne/, Accessed: 2025-09-02, 2025.

[3] International Moth Class Association, *International moth class rules*, Dec. 2024. [Online]. Available: https://www.sailing.org/classes/moth/#Documents.

[4] International Hydrofoil Society, *Aeromarine origins — early work by thomas moy (1861)*, Online article, Accessed 7 Sep 2025, 2018. [Online]. Available: https://www.foils.org/wp-content/uploads/2018/01/AeromarineOrigins.pdf.

[5] International Hydrofoil Society, *Ships that fly — forlanini's hydrofoil on lake maggiore (1906)*, Online booklet, Accessed 7 Sep 2025, 2018. [Online]. Available: https://www.foils.org/wp-content/uploads/2018/01/ShipsThatFly.pdf.

[6] Alexander Graham Bell Foundation, *Hydrofoil history: Bell and baldwin's hd–4*, Web page, Accessed 7 Sep 2025, 2024. [Online]. Available: https://agbfoundation.ca/hydrofoil/.

[7] The Canadian Encyclopedia, *Hydrofoil (historical overview and hd–4 record)*, Web page, Accessed 7 Sep 2025, 2023. [Online]. Available: https://thecanadianencyclopedia.ca/en/article/hydrofoil.

[8] T. M. Buermann, "An appraisal of hydrofoil supported craft," *SNAME Transactions*, vol. 61, 1953. [Online]. Available: https://www.foils.org/wp-content/uploads/2018/01/SNAMEtransactionsVol61-1953.pdf.

[9] E. D'Amato *et al.*, "Hydrodynamic design of fixed hydrofoils for planing craft," *Journal of Marine Science and Engineering*, vol. 11, no. 2, p. 246, 2023. DOI: 10.3390/jmse11020246. [Online]. Available: https://www.mdpi.com/2077-1312/11/2/246.

[10] L. Larsson, R. E. Eliasson, and M. Orych, *Principles of Yacht Design*, 5th. London: Adlard Coles / Bloomsbury, 2022, ISBN: 9781472981929.

[11] J. I. R. Blake, *Lecture notes on sess3027 yacht & high performance craft*, Lecture notes, 2021.

[12] F. Fossati, *Aero-hydrodynamics and the Performance of Sailing Yachts: The Science Behind Sailing Yachts and Their Design*. London: A & C Black Publishers Ltd, 2009, p. 352, ISBN: 9781408113387.

[13] B. Beaver and J. Zseleczky, "Full scale measurements on a hydrofoil international moth," in *SNAME Chesapeake Sailing Yacht Symposium*, 2009, D021S002R006.

[14] Maguire Boats Ltd. "Main foil parts." Product category page; photograph retrieved by author, Maguire Boats Ltd. (), [Online]. Available: https://maguireboats.com/main-foil-parts-23-c.asp (visited on 09/06/2025).

[15] F. Eggert, "Flight dynamics and stability of a hydrofoiling international moth with a dynamic velocity prediction program (dvpp)," M.S. thesis, Technische Universität Berlin, 2018.

[16] J. E. Kerwin, "A velocity prediction program for ocean racing yachts," *Rep 78-11 MIT*, Jul. 1978.

[17] A. R. Claughton, J. F. Wellicome, and R. A. Shenoi, *Sailing Yacht Design: Theory*. Harlow: Addison Wesley Longman, 1998.

[18] A. R. Claughton, "Developments in the ims vpp formulations," in *Proceedings of the 14th Chesapeake Sailing Yacht Symposium*, SNAME, Annapolis, MD, 1999.

[19] *Orc vpp documentation*, Technical description of the ORC Velocity Prediction Program, Offshore Racing Congress, 2020. [Online]. Available: https://www.orc.org/rules/.

[20] P. Kerdraon, B. Horel, P. Bot, A. Letourneur, and D. Le Touzé, "Development of a 6-dof dynamic velocity prediction program for offshore racing yachts," *Ocean Engineering*, vol. 212, p. 107 668, 2020. DOI: 10.1016/j.oceaneng.2020.107668.

[21] D. P. J. Hull, "Speed sailing design & velocity prediction program," BEng thesis, Australian Maritime College, University of Tasmania, 2014.

[22] N. Patterson and J. Binns, "Development of a six degree of freedom velocity prediction program for the foiling america's cup vessels," *Journal of Sailing Technology*, vol. 7, no. 1, pp. 120–151, 2022.

[23] A. Persson, "Predicting yacht performance in waves using a cfd velocity prediction program," Ph.D. dissertation, Chalmers University of Technology, 2025.

[24] R. Tannenberg, S. R. Turnock, K. Hochkirch, and S. W. Boyd, "Vpp driven parametric design of ac75 hydrofoils," *Journal of Sailing Technology*, vol. 8, no. 1, pp. 161–182, 2023.

[25] L. Sampedro Moix, "Preliminary design of a racing dinghy: F18 catamaran," B.S. thesis, EPEF, Universidade da Coruña, 2023.

[26] S. Day, L. Letizia, and A. Stuart, "Vpp vs ppp: Challenges in the time-domain prediction of sailing yacht performance," in *Proceedings of the High Performance Yacht Design Conference (HPYD 1)*, Conference dates: 4–6 December 2002, Auckland, New Zealand: Royal Institution of Naval Architects (RINA), 2002. DOI: 10.3940/rina.ya.2002.07.

[27] D. H. Harris, "Time domain simulation of a yacht sailing upwind in waves," in *Proceedings of the 17th Chesapeake Sailing Yacht Symposium*, Annapolis, MD, USA: SNAME, Chesapeake Section, 2005, pp. 13–32.

[28] H. Hansen and et al., "Maneuver simulation and optimization for ac50 class," in *Journal of Sailing Technology*, 2019. [Online]. Available: https://higherlogicdownload.s3.amazonaws.com/SNAME/1516f098-2760-4bff-86fa-9ca63a85f102/UploadedImages/2019-07__Hansen_et_al__Maneuver_Simulation_and_Optimisation_for_AC50_Class.pdf.

[29] M. F. Melis, "Velocity prediction program for a hydrofoiling lake racer," *Journal of Sailing Technology*, 2022. [Online]. Available: https://www.foils.org/wp-content/uploads/2022/08/Melis-Submission-Hamburg-University-Honorable-Mention.pdf.

[30] K. Hochkirch, *Fs-equilibrium user manual*, Citado por Tannenberg (2023) como manual de referencia de FS-Equilibrium, DNV GL Maritime, 2018.

[31] M. Brito, "Use of gomboc to predict the performance of a hydro-foiled moth," Yacht Research Unit, The University of Auckland, Tech. Rep., 2019.

[32] Simulator in Motion. "Demonstration video (homepage)." Frame captured by the author for academic illustration. (), [Online]. Available: https://www.simulatorinmotion.com/ (visited on 09/07/2025).

[33] Redondo Studio. "Redondo studio portfolio: Moth." Photo captured by the author for academic illustration. (), [Online]. Available: https://redondo.studio/portfolio/moth2024 (visited on 09/07/2025).

[34] K. Graf, O. Freiheit, P. Schlockermann, and J. C. Mense, "Vpp-driven sail and foil trim optimization for the olympic nacra 17 foiling catamaran," *Journal of Sailing Technology*, vol. 5, no. 01, pp. 61–81, 2020.

[35] M. Jardine. "Unboxing the bieker moth with kyle stoneham," Sail-World. (Sep. 6, 2025), [Online]. Available: https://www.sail-world.com/news/289699/Unboxing-the-Bieker-Moth-with-Kyle-Stoneham (visited on 09/09/2025).

[36] L. Llamas. "Adjust pid controller on arduino." Accessed: 2025-08-25. (2023), [Online]. Available: https://www.luisllamas.es/en/adjust-pid-controller-arduino/.